A Non-Destructive Transformer Oil Tester

by

Timothy L. Cargol

Submitted to the Department of Electrical Engineering and Computer Science

in Partial Fulfillment of the Requirements for the Degree of

Master of Engineering in Electrical Engineering and Computer Science

at the

MASSACHUSETTS INSTITUTE OF TECHNOLOGY

May 2000

[June 2000]

Author_____
Department of Electrical Engineering and Computer Science
May 2000

Certified by_____
Chathan M. Cooke
Thesis Supervisor

Accepted by_____
Arthur C. Smith
Chairman, Department Committee on Graduate Theses

A Non-Destructive Transformer Oil Tester
by
Timothy L. Cargol

Submitted to the
Department of Electrical Engineering and Computer Science

May 2000

In Partial Fulfillment of the Requirements for the Degree of
Master of Engineering in Electrical Engineering and Computer Science

ABSTRACT

A new non-destructive test of transformer oil dielectric strength is a promising technique to automate and make more reliable a diagnostic that presently involves intensive manual efforts. This thesis focuses some of the issues that must be understood to bring the test from the laboratory to the field. Emphasis is placed on reliability and safety by exploring any effect the test has on the transformer oil, the mechanical parameters necessary to give optimal reliability, and failsafe electronics.

Thesis Supervisor: Chathan M. Cooke
Title: Lecturer, Department of Electrical Engineering and Computer Science, and Principal Research Engineer, M.I.T. Laboratory for Electronic and Electromagnetic Systems

Table of Contents

List of Figures

Chapter 1

Introduction

The electric power transformers used in virtually every substation throughout the world are cooled and electrically insulated by oils. Over time, through the changing of taps, absorption of moisture and gasses, the transformer oils will degrade and no longer provide adequate electrical insulation. The process of degradation can take anywhere from months to years, but when the oil is found to be weak or bad, immediate action must be taken to clean or replace the oil. Oil failure in a multi-million dollar 230kV transformer can be quite expensive and dangerous, so an accurate measure of condition of the oil is very valuable to the electric utilities.

Oil testing reduces the risk of transformer failure. Presently, the process for testing the oil costs electric utilities a considerable amount time and money. It is necessary to send a technician out to every transformer at each substation to test the condition of the oil. Often traveling 50 miles or more to reach the substation, the technician typically withdraws up to 2 Liters of oil into highly cleaned bottles or syringes. [1] The oil is then packaged up and sent off to an analytical lab. The results of the test can take several weeks to be returned and the oil is destroyed in the process of testing.

1.1 Present Test Method, ASTM

The most important measure of a transformer's oil condition is its breakdown (or dielectric) strength. The breakdown strength is the level of electrical stress at which the oil will stop insulating and breakdown, letting current flow through it. The most common measures of the dielectric strength are the ASTM D-877 [1] and D-1816 tests. Both tests measure breakdown strength by applying a steadily increasing AC voltage between two electrodes. The disk-like (D-877) or rounded (D-1816) electrodes are placed about 1mm apart and the voltage across them is increased at 3kv/second until a breakdown occurs. At that point the voltage is shut off within a cycle or so and its value at breakdown is recorded. A complete D-877 test consists of five shots with this procedure and the result is the average of the breakdown voltages. After 5 D-877 shots the oil has been too damaged for any more tests and cannot be returned to the transformer.

Damage to the oil results from the tremendous amount of electrical energy that is dumped into the oil before the test voltage is shut off. The ASTM test apparatus must actively sense when a breakdown has occurred and shut off the many tens of kilovolts of test voltage. The process of sensing and shutting off the voltage is inevitably too slow to prevent oil damage, and as it is an active process, could never be depended on for reliable prevention of oil damage.

1.2 NDBD Test

A new test developed by Dr Chathan Cooke at M.I.T. [2] has the potential to offer nondestructive breakdown testing and in-situ testing. Unlike the ASTM tests, the nondestructive breakdown test (NDBD) requires only a tiny amount of oil and subjects it to an extremely short 300ns pulse of electrical stress. In the test, a 300ns high voltage pulse of 20kV to 35kV is applied across a point to plane gap of .005-.020 inch. In perfect oil no breakdown will occur and the test is completely nondestructive. In degraded oil some micro-breakdown events will occur. These micro-breakdown events are of such an

infinitesimal scale compared to ASTM methods, that the NDBD test is for all practical purposes nondestructive. [Fig. 1-1]

By measuring the number of breakdowns that occur and their time until breakdown during the 300ns pulse, conclusions can be drawn about the condition of the oil. There is a very strong correlation between both the number and time of breakdowns and the known quality of the oil. Data has shown that as oil quality decreases the time until breakdown also decreases. The time until breakdown will also decrease as the voltage increases.

a)

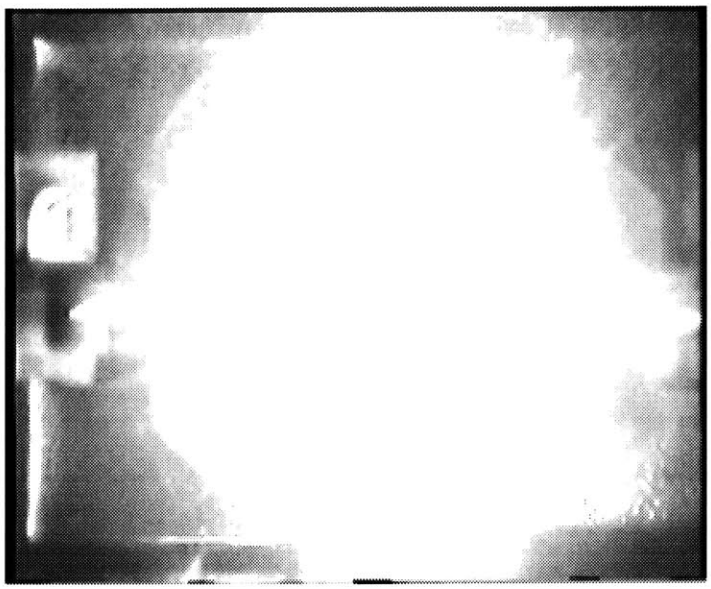

b)

Figure 1-1 Equal scale video frame images of a) breakdown in D-877 test, and b) NDBD test. Consult Appendix A for more images of D-877

The NDBD test can be relied upon as non-destructive because of the way the 300ns pulse is delivered. Instead of a large high-voltage transformer capable of delivering steady current, the NDBD test uses a transmission line type pulser to deliver the high voltage pulse. [Chapter 3] Even if all of the high voltage components fail, the pulser can only deliver 300ns of high voltage. Through this choice of pulser, and careful design of the testing gap and external components, the NDBD test can be depended upon for safe and reliable service in the field; and hence connected directly to a live transformer. The

major components of the NDBD test apparatus include the pulser, the test gap, and data acquisition, as diagramed below:

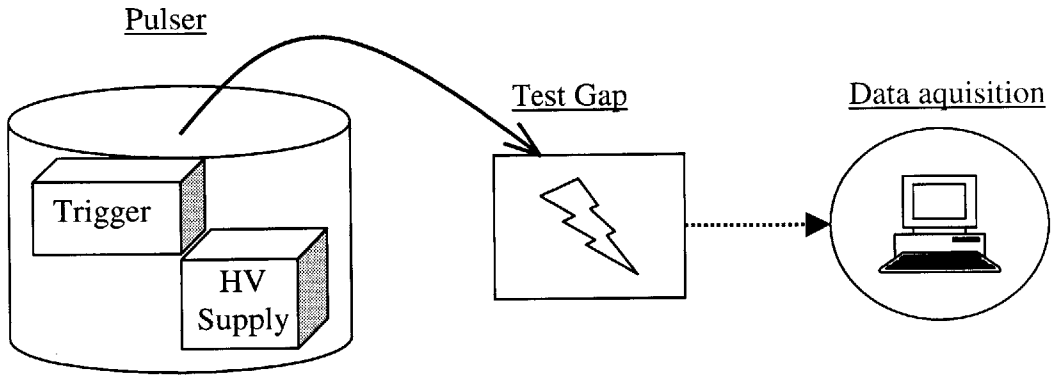

Figure 1-2 Overall System Architecture

1.3 Emphasis of This Thesis

This thesis focuses on some of the issues that must be investigated to bring the NDBD tester from the lab bench to the field. Chapter 2 explores the nature of the oil breakdown in the test gap. A model for effects on the oil is proposed and evaluated through extensive experiments to establish important factors that quantify breakdown events. These results are used to recommend the design of test gaps. Chapter 3 discusses the electronics necessary to drive the test, focusing on the design of the pulser itself, reducing it from a cumbersome laboratory apparatus to a compact unit rugged enough to be bolted to a transformer. Chapter 3 also looks at data acquisition, and ways that the oscilloscope and computer may be replaced by simple electronics. Overall system results are presented in chapter 4, and a summary of this thesis is given in chapter 5. As the eventual goal is to apply the NDBD test is to an in-service transformer, the design and evaluation of the NDBD tester was made with the following parameters in mind:

Functional Requirements

- Non-Destructive. Any effects on the oil must be minimized
- Accessible to the oil. The probe must be arranged to immerse the test gap in the transformer oil
- Effective Pulser. Pulses must be clean and reliable
- Simple data acquisition.

Practical Requirements

- Inexpensive
- Compact

Chapter 2

The NDBD Micro-Discharge

The NDBD test has been shown to be an effective means to distinguish between good and degraded oils in the laboratory. However, to make the transition to the transformer yard requires some further investigation into the physics of the test. Utilities are very concerned with any equipment that could potentially harm the transformer oil and so any effects resulting from the NDBD test must be understood and controlled to be negligible. This chapter proposes a model for the micro-discharge process in the oil and explores what mechanical and electrical parameters are necessary to minimize any potential effects from the NDBD test.

2.1 Point to Plane Gap Structure

Previous work with the NDBD system had found that a negatively pulsed needlepoint to plane gap provided the most sensitivity to oil condition. [2,3] This configuration was again verified to provide the best sensitivity by testing oils in various conditions. The negatively pulsed point to plane test gap was used in all NDBD work in this thesis.

2.1.1 Mechanical criteria

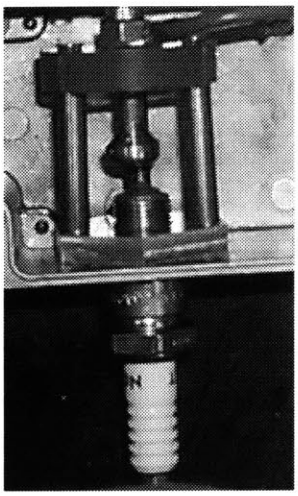

Figure 2-1 Thermally Stabilized Probe

To make a test gap that will provide many thousands of shots of reliable service requires some careful mechanical consideration. In the harsh environment of an outdoor substation thermal stability is important to maintain gap performance. Conditions can range from a freezing artic winter to the heat of an over loaded transformer on a record breaking hot day. All the while, the test gap must maintain its proper spacing to better than 0.001". For test cells in the lab, this criteria was not so easily evaluated, however a thermally stable version has been constructed. [Fig. 2-1] To keep thermal expansion in check, the plane spacing material is the same as the point material. By this arrangement the net thermal expansion of the test gap essentially cancels.

Selection of electrode material is also an important consideration. The material must not erode excessively, and not become fouled with any deposits that would hinder performance. In an early test cell brass was used for the plane electrode and stainless steel for the needle point. [Fig. 2-2] Both these materials are not easily eroded, yet after several thousand shots some wear patterns could be seen. Fortunately, the wear results in a slight blunting of the electrode tip. The radius of the tip increases from erosion, and so more and more material must be removed to further change the radius. Erosion begins to asymptotically slow at about 100 μm.

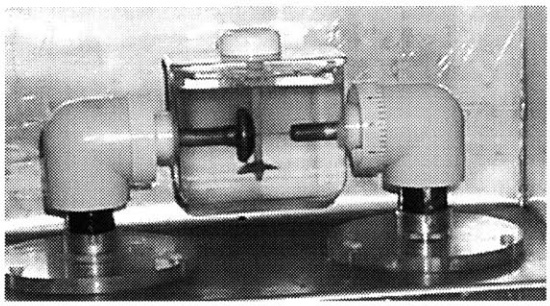

Figure 2-2 Point to plane cell from early NDBD system

2.1.2 Tip Geometry

With each breakdown event a microscopic amount of material is worn off the electrode. As can be seen in Figure 2-3, the wear of many thousands of shots begins to create an erosion pattern on the plug tip. This erosion pattern must be understood and optimized for two reasons. First, as the erosion grows up the conical point of the plug, the tip radius increases. Increasing the tip radius decreases the concentration of the electric field at the tip, thus possibly desensitizing the test. The second reason erosion must be optimized, is that it shortens the length of the point, widening the gap spacing. If the gap spacing increases substantially, the pulse voltage must be increased to compensate. Erosion of both the tip radius and the tip length needs to be minimized, and as it turns out, they are inversely related so an ideal operating point can be found.

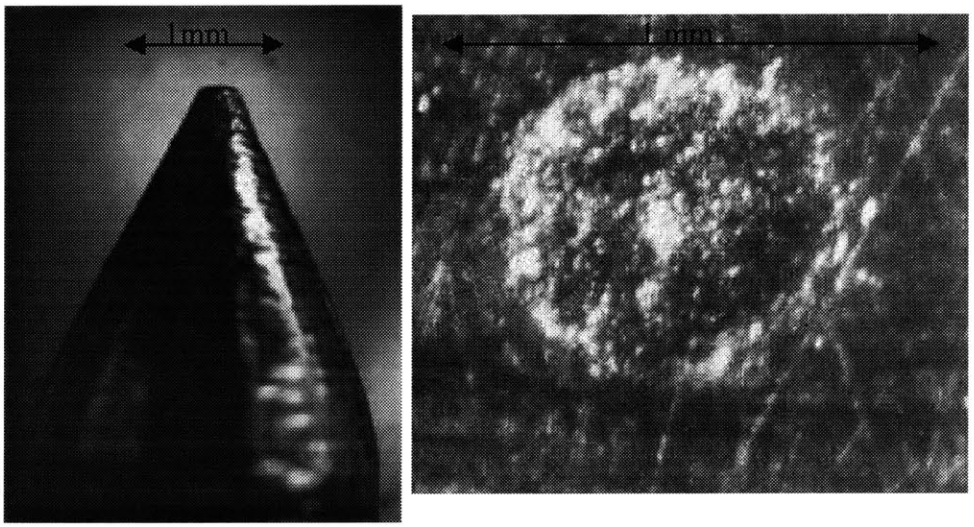

Figure 2-3 Electrode rounding and plate pitting after several thousand shots

The geometry of the eroded tip can be visualized as a truncated cone with a spherical top. The actual tip may be an oblate spheroid, ellipsoid, or some other complex shape, but it basically resembles a sphere, which is a close enough approximation. The volume that has been eroded is then the volume contained within cone and bounded on the bottom by a tangentially nested sphere. [Fig. 2-4] The height that has been lost to erosion is the line from the tip of the cone to the top of the sphere. The volume of material eroded from the tip is calculated via:

$$V = \tfrac{1}{3}\pi\alpha^2 h - \tfrac{2}{3}\pi R^3 + \alpha^2\pi\sqrt{R^2-\alpha^2} + \tfrac{2}{3}\pi\left(R^2-\alpha^2\right)^{3/2}$$

$$\alpha = R\cos\tfrac{1}{2}\theta, \quad h = \frac{R\cos\tfrac{1}{2}\theta}{\tan\tfrac{1}{2}\theta}$$

Where R is the tip radius (radius of nested sphere) and θ is the cone angle. A complete derivation will be omitted here, but is included in appendix B. The eroded volume is a function of tip radius and cone angle and is plotted on the x-axis in figures 2-5 and denoted by the dashed curves in figure 2-6.

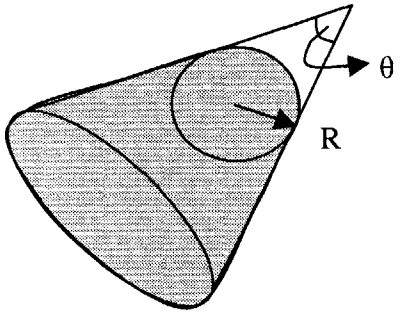

Figure 2-4 Geometric model for tip erosion

Assuming that the electrode material erodes at a constant volume per shot, the only variables that will make a difference in the erosion characteristics are the cone angle, and any pre-rounding of the tip that is done. Figure 2-5 shows the rounding of the tip as a function of the volume of material lost for different tip angles. Figure 2-6 shows the shortening of the point as a function of the tip height lost for different tip angles. Since the erosion of material is assumed to be a static function of the number of shots, the x-axis of figure 2-5 and the dashed curves of figure 2-6 can also be viewed as the number of shots instead of a volume. The amount of material removed per shot does not need to be known to determine the optimal geometry as long as the volume per shot is consistent. Different materials will wear at different rates, but regardless of the rate, the optimal shape dictated by the geometric model will be the same.

As can be seen in the graphs, a narrow tip angle will maintain a constant radius over many shots better than a shallow tip angle. A shallow tip angle however will minimize shortening of the tip. Looking at the graphs, a tip angle of about 30° is a good compromise between the two criteria. Pre-rounding the tip to a radius of about 100-150

μm will also bypass the steepest part of the wear curves. With a 30° cone angle the first 10^7 μm^3 of material eroded changes the tip radius changes from 0 to 150 μm. When the next 10^7 μm^3 of material is eroded, the tip radius only increases to 200μm. A typical shot may erode 10 μm^3 of material. The modified NGK plugs had a cone angle of 40° and through several thousand shots had a tip radius of about 100μm.

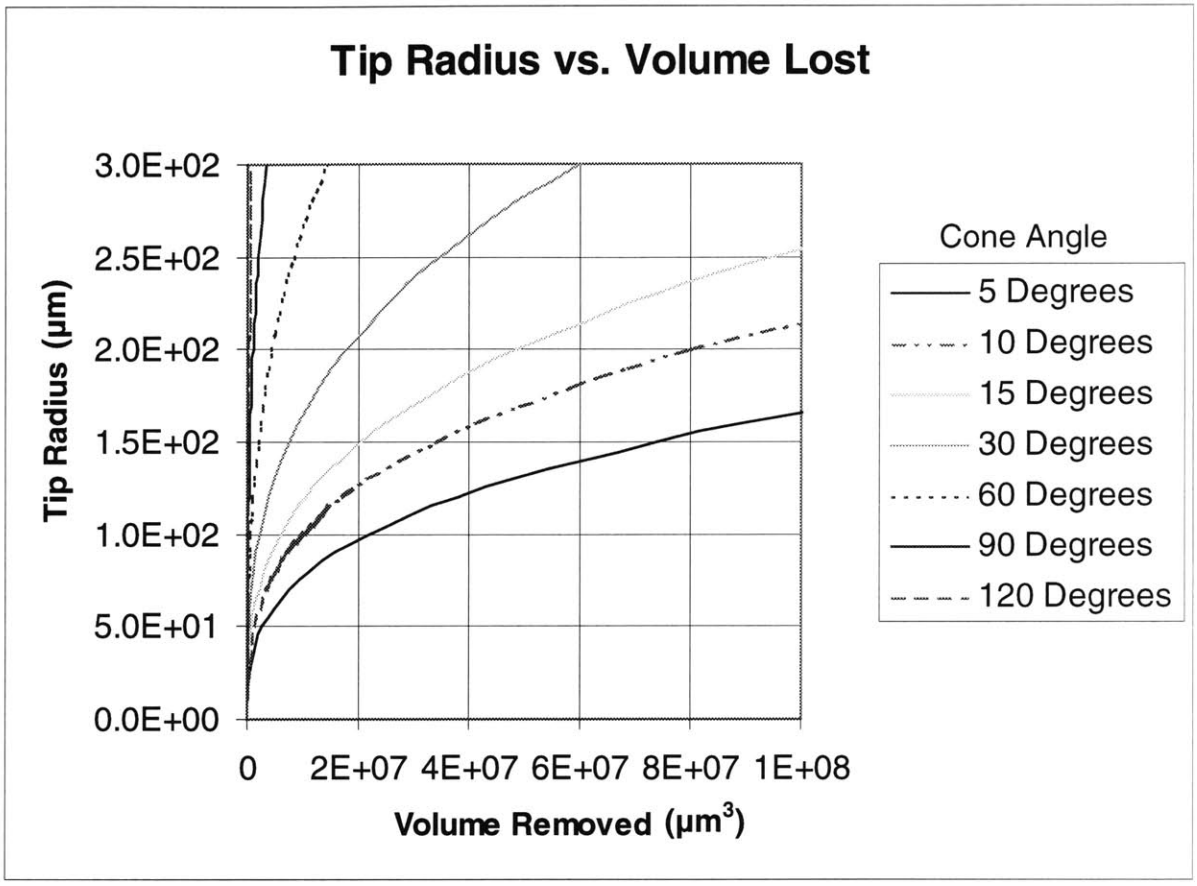

Figure 2-5 Tip radius as a function of volume removed. The x-axis can also be viewed as the number of shots.

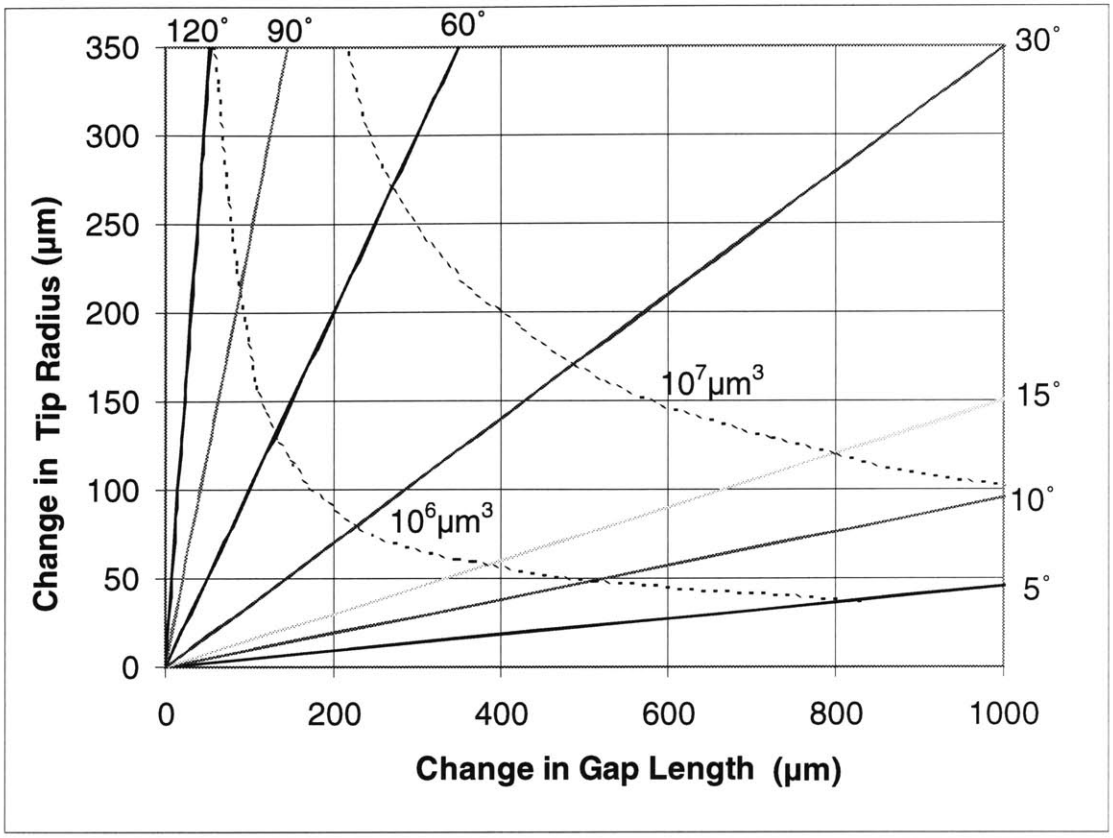

Figure 2-6 Change in tip radius as a function of change in gap length for various angles.

2.1.3 Spark Plugs

Spark plugs have several features that would make them an ideal ready-made solution for many of the design criteria of the test gap. Firstly, they are made to seal and not leak against high engine pressures and temperatures and hence could screw directly onto a transformer tank without leaking. Secondly, they incorporate a rugged ceramic insulator designed to insulate against many tens of kilovolts for years of service, so the pulse voltage insulation is not a problem. Thirdly, the electrode is coated with platinum or made of other erosion resistant materials and is thermally stable for a long life of millions of sparks. Finally, they come in a large variety of shapes and sizes. Unfortunately however, a ready made point to plane spark plug suitable for NDBD tests has yet to be found and appears not to be a standard item.

Various stock plugs have been tested, but none has yielded satisfactory performance in the off the shelf condition. The test voltages in the present pulser are set to 20-25 KV, so achieving breakdowns requires relatively short gap spacing. The factory gap for a spark plug, or the gap most commonly used in a car, is about .030". For the NDBD tests, gaps of .005"-.010" were used with best results occurring around .006". With this much smaller gap spacing the blunt faces of standard spark plugs more closely approximate a plane-to-plane gap. Needless to say, the results of short gapped stock spark plugs were not very reliable. With large blunt faces debris could remain trapped between the large electrodes by surface tension and facilitate repeated breakdowns.

Despite the shortcomings of off the shelf plugs, spark plugs are still quite promising. To create a more point to plane like plug, the plug's arm can be machined off. Then with the arms removed the center electrode can be easily machined to a fine point. Various types of external planes can be added to replace the ground return of the plug's arm. A reliable combination consists of a modified NGK BP6ET plug perpendicular to a small brass plate. The NGK plug has the longest and therefore most easily machined center electrode of all the plugs examined. After machining, the space between the ceramic insulator at the tip of the plug and the metal jacket was filled with an oil resistant RTV to prevent entrapment of gasses or air along the insulator. [Fig. 2-7]

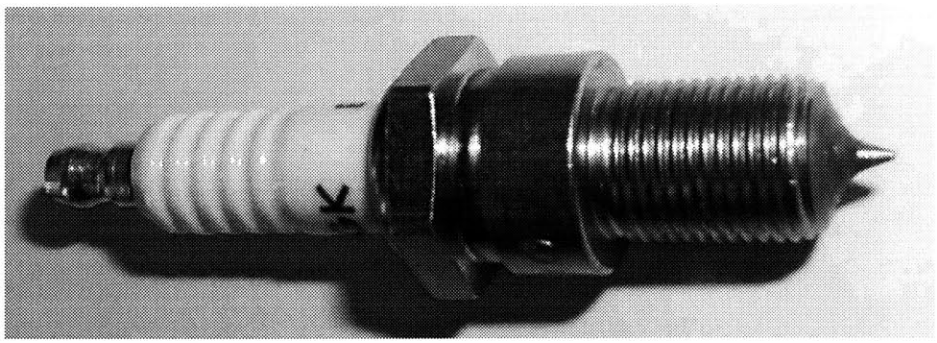

Figure 2-7 Picture of modified spark plug

2.1.3.1 Electrical Circuit Parameters of Spark Plugs

While the NGK plug resembles the point to plane gap mechanically, there are notable electrical differences. To enable plugs to screw tightly into the engine head and withstand combustion pressures, spark plugs have a metal jacket tightly encasing the ceramic core. This metal jacket adds a considerable amount of parallel capacitance to the gap, measured at about 12pf for the NGK plug. This extraneous capacitance slows the rise time of the pulse and adds stored energy that can dump through the oil when it breaks down.

The conductive core of the spark plug also has some inductance. While it was too low to accurately measure with available equipment, the spark plug inductance could be readily calculated from its geometry. [4] Modeling the core as a straight wire, the inductance will be:

$$L = 0.129\ell\left[2.303\log_{10}\left(\frac{4\ell}{d}\right) - 0.75\right] \quad \ell \text{ and } d \text{ are in meters, } L \text{ is in } \mu H$$

For the measurements of the NGK BP6ET, this yields approximately 0.03 μH.

The inductance and capacitance of the spark plug [Fig. 2-8] form a series RLC network and cause it to ring when excited by a breakdown. Figure 2-9 shows the voltage on the tip of the plug with different capacitances added in parallel to the 12pf of the NGK plug. The added capacitance helps to both demonstrate the effect of capacitance on slowing the rise time, and to lower the ring frequency below the bandwidth of the probe used to measure it.

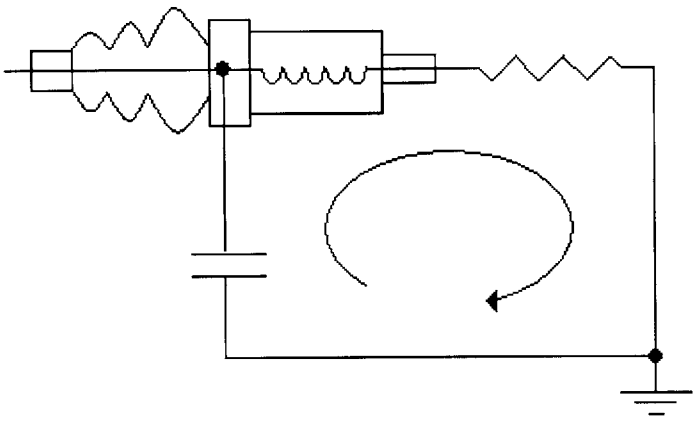

Figure 2-8 Circuit Diagram of Oscillations Due to Plug Inductance and Capacitance

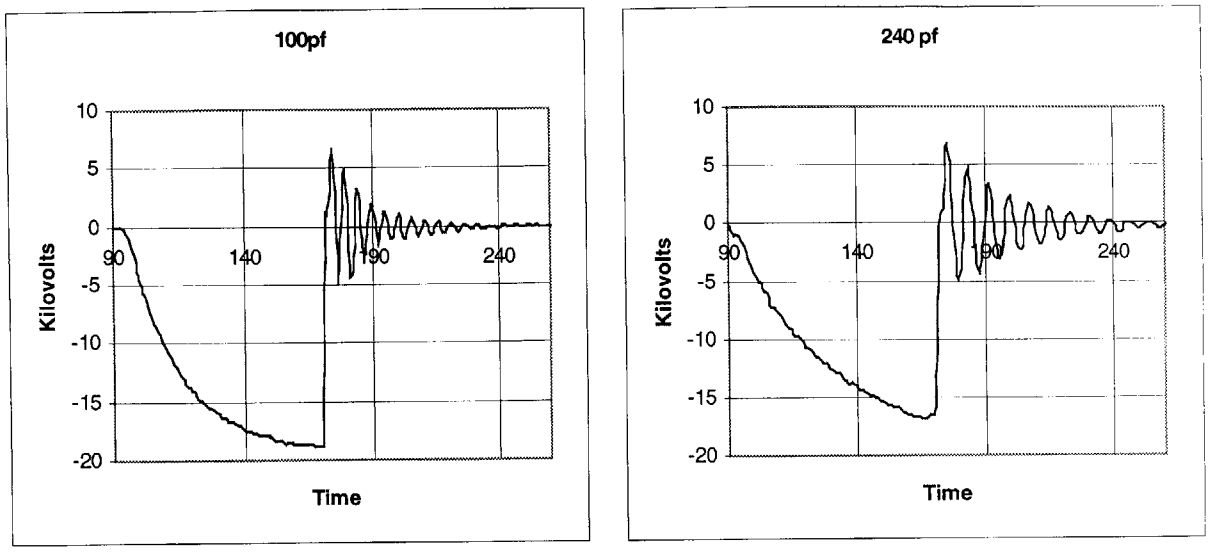

Figure 2-9 Voltage on Plug Tip with Different Parallel Capacitances. Note slower rise time and lower ring frequency with 240pf

2.2 Micro-Discharge Event in Oil

While it has already been shown that thousands of NDBD shots produce no detectable damage to the oil, [2] it is speculated that some effects in the oil could result from the short NDBD pulse. Possible causes for effects in the oil could be the current traveling through the oil, the energy dissipated in it, or the voltage stress on it. This section explores the relationship between currents, voltages, and measurable effects in the oil.

2.2.1 Experimental Set-Up

In order to create a more realistic transformer-like environment for the test probe, a test gap was positioned at the end of an aluminum tube inside a heavy gauge steel box, similar to the mounting that would be used on an actual transformer. [Fig. 2-10] Inside the box the tip of the plug sits immersed in a square polycarbonate vessel filled with oil. The polycarbonate vessel is square so that a video camera, with a 25X macro lens can record the breakdown events without distortion. Voltage measurements are taken with a Tektronix P6015A 75MHz 40Kv probe, and current was measured via a 0.1Ω precision low inductance resistor connecting the aluminum cylinder (which the plug screws into) to

ground. Both voltage and current probes are connected to a Tektronix TDS 540A 500MHz 4-channel scope.

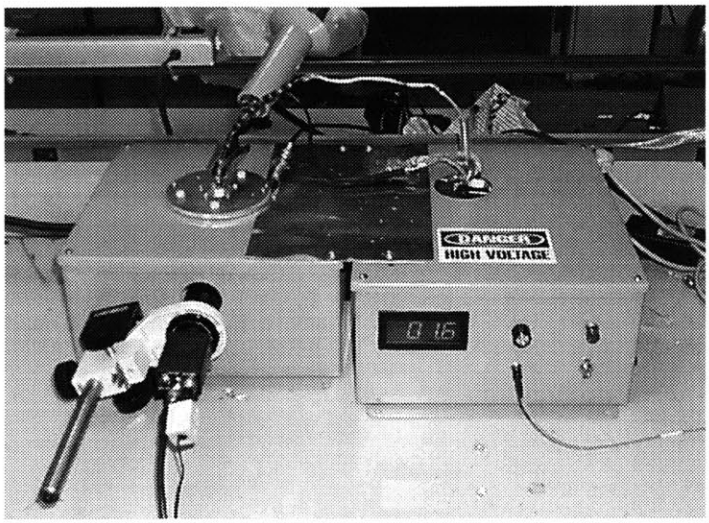

Figure 2-10 Picture of Setup Used

Test gap in box at left (with video camera in foreground), pulser box on right

Measurements were made on oil taken from a transformer located at a substation called Gretna. This "Gretna" oil was chosen because it was degraded and therefore allowed consistent breakdowns with a .006" gap in the 20-25Kv range of the pulser. Gretna was also relatively clear and so would allow video images of breakdown events. The tests were performed on this one type of oil with the same gap spacing in order to eliminate those variables in trying to create a model of the breakdown process in the NDBD test. It will be assumed that while the specific results of tests with different oils and different gaps may be different, the underlying physics will be similar.

Test shots were made in series of 20 shots, 30 seconds apart. The voltage and current waveforms were recorded along with the video images. Figure 2-11 depicts the equivalent electrical circuit for the basic test system. Test conditions were varied, including changing the series resistance (R2) to the test gap, and the pulser voltage (either 20 or 24 Kv). An extra capacitance positioned between the top of the spark plug and ground (C4) could be added to alter the energy flow and the resonant frequency of the network.

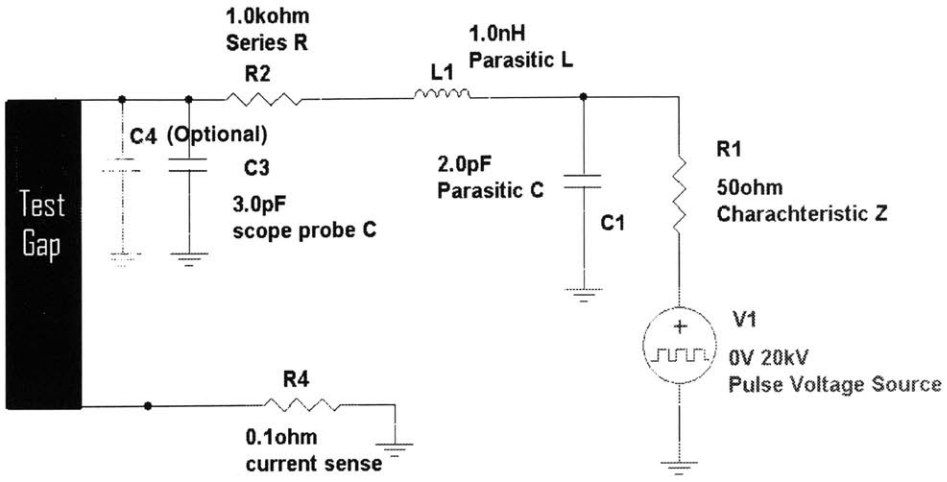

Figure 2-11 Circuit diagram of setup

2.2.2 Typical Micro-Discharge Event

The voltage across the gap and current through the test gap are depicted in figure 2-12 along with the video images of a typical micro-discharge event shown in figure 2-13. For these, the pulse is 24kV, 300nS long and incorporated 150Ω total series resistance (R1+R2=150), (C4=0). Some observations that can be noted are:

1) The high peak current in the current plot
2) The steady "on" state current after the ringing
3) The plug capacitance charging current seen at the beginning of the pulse
4) A single frame of very localized light emission observed due to the persistence of the video imagery
5) The ejection of gas in the video sequence

Figure 2-12 Voltage and current waveforms for a sample NDBD micro-discharge event ↓

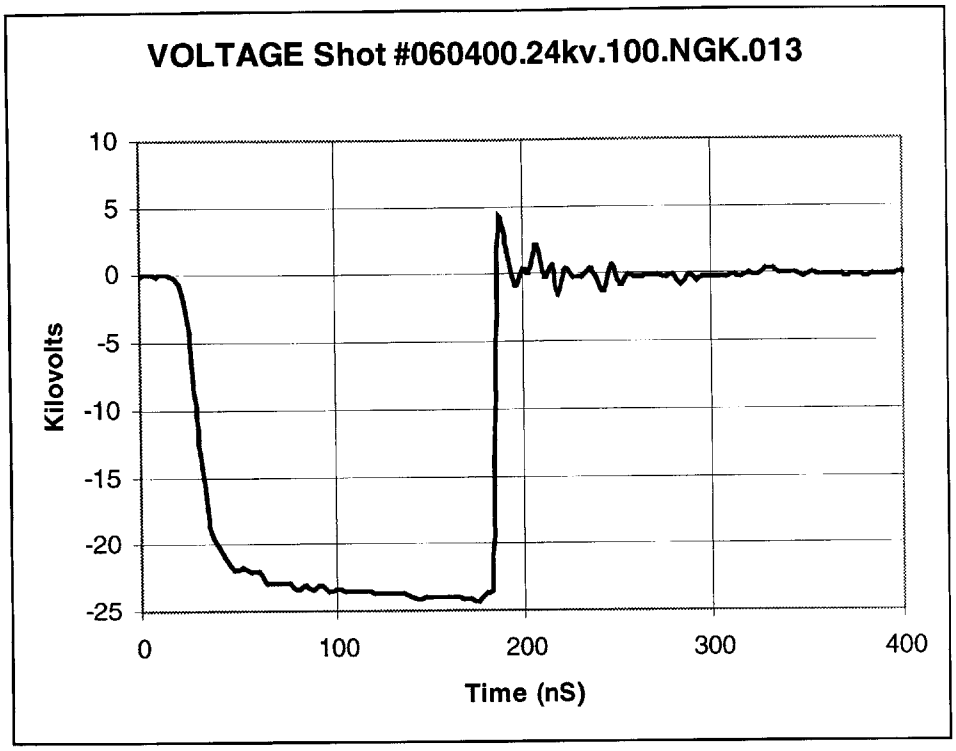
VOLTAGE Shot #060400.24kv.100.NGK.013
Kilovolts
10
5
0
-5
-10
-15
-20
-25
0
100
200
300
400
Time (nS)

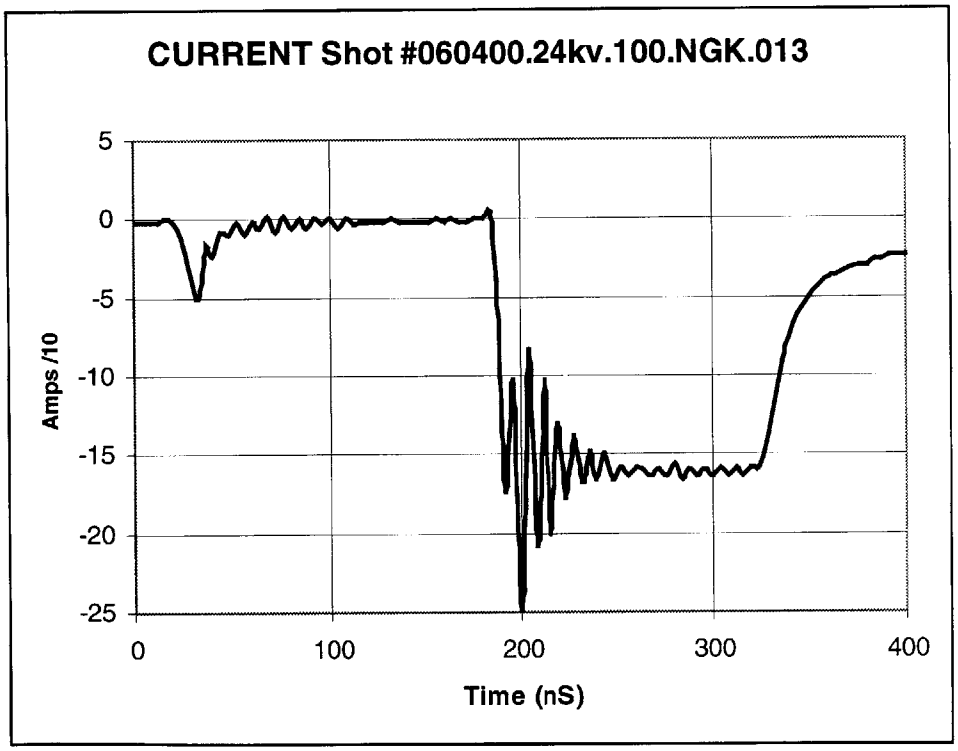
CURRENT Shot #060400.24kv.100.NGK.013
Amps /10
5
0
-5
-10
-15
-20
-25
0
100
200
300
400
Time (nS)

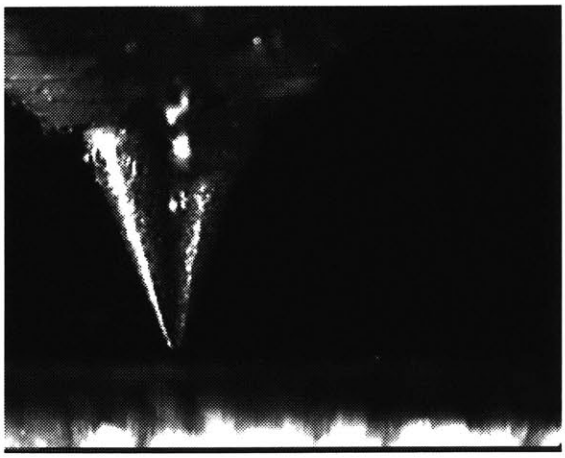

Time = -33ms, before breakdown

Time = 0ms, breakdown

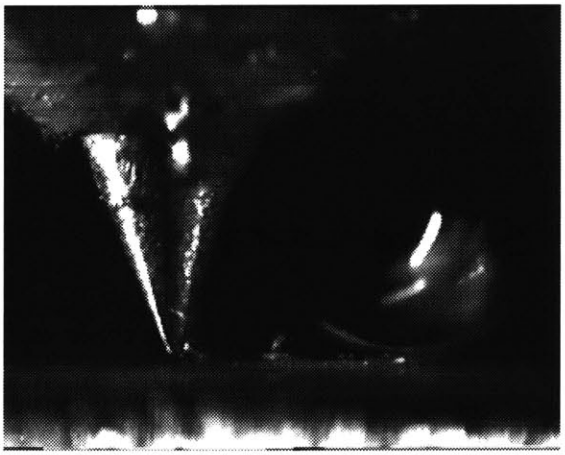

Time = +33ms

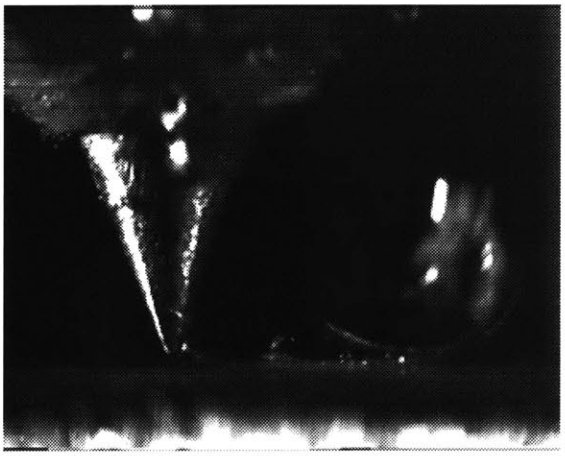

Time = +66ms

Time = +200ms

Figure 2-13 Video Sequence of typical micro-discharge event

2.2.3 Resistive Energy Losses in the Oil

One possible cause of change in the oil is the resistive energy dissipated in the oil. Previous research has shown that there are 2 main phases of breakdown in an oil gap. [5,6] [Fig. 2-14] First there is the transition region where the channel is highly resistive and considerable power is dissipated in the channel. Then the gap settles to a lower "on" state resistance. Measurements to determine the time the gap spends in the highly resistive state were unsuccessful because it was much too fast for the equipment to measure. [Fig. 2-12] The transitions happened in under 2ns, beyond the bandwidth limit of the scope probe. Since the transitions were un-measurable and very short in comparison to other significant times, energy dissipated during the transitions will be not be considered in the model.

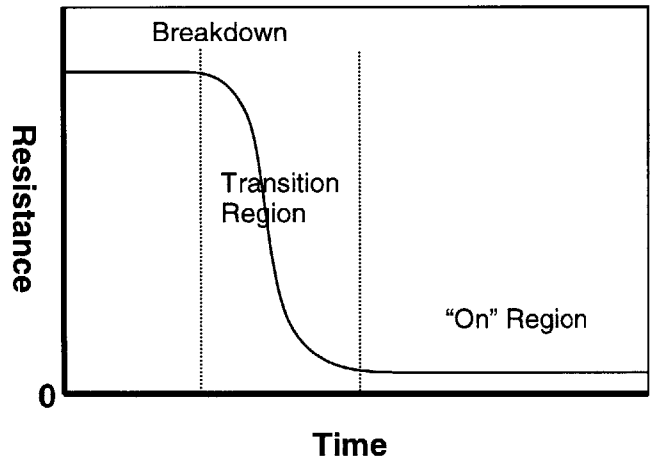

Figure 2-14 Resistance During Breakdown

2.2.3.1 Determination of test gap electrical parameters

Finding the "on" state resistance is not as simple as using Ohm's law and just measuring the voltage across the gap and the current through it. A thorough model of the test gap, including the spark plug and mechanical connections had to be constructed in order to fully understand the measured voltage and current waveforms. Figure 2-15a shows the circuit diagram of the test gap and plug. The diagram includes all the virtual and real components from the series resistors on the terminal of the spark plug to the junction with the ground return to the pulser. Excluding R3, the external series resistance and R2 the current sensing resistor, this circuit represents the test gap "black box" seen in figure 2-11. Some of the components such as the series resistance are known. Others such

as the plug capacitance can be directly measured. The remaining components must be estimated or indirectly measured. Table 1 summarizes the measured or estimated values of all the components in the model.

While it does take all of the virtual components into account, the circuit of figure 2-15a is more complicated than is needed to provide a good model that fits the measured data. A simpler model is shown in figure 2-15b. Looking at the estimated component values in table 1, several components are small enough to be neglected and others can be combined. The arc inductance and tip to plane capacitance are much smaller than the other inductances and capacitances and are thrown out. The plug inductance and capacitive return inductance are combined, as are the plug capacitance and the assembly capacitance. The resulting circuit is simply a series *RLC* loop with *C* a measurable quantity, and *L* split by the ground point. While this circuit is visibly less sophisticated than the full model, it provides a good enough match to the measured results, and it makes *R* and *L* possible to extract from the data. *R* and *L* were estimated from the data in 3 separate ways:

1) Adding external parallel capacitors and examining the effects on ring frequency
2) Digitally filtering the current waveform to enable the extraction of a value for R
3) Using the current data to generate a bode plot for the system function

The arc inductance was calculated with the inductance formula in section 2.1 using dimensions estimated from video observations. The location of the split in the series inductor in the simplified model could only be calculated and estimated by comparing simulated traces against the actual. A calculation of the upper inductance (L02) is based on the dimensions of the metal jacket tube surrounding the spark plug's ceramic core. $L = \frac{\mu}{2\pi} \ln \frac{b}{a}$ [11] Where *L* is per unit length, *a* is the radius of the plug core, and *b* is the radius of the surrounding metal jacket. From these calculations, the estimated upper inductance equals about 100nH for the dimensions of the plug and tube. Using this calculated value in a P-SPICE simulation results in waveforms that nearly match the measured waveforms. [Fig. 2-17]

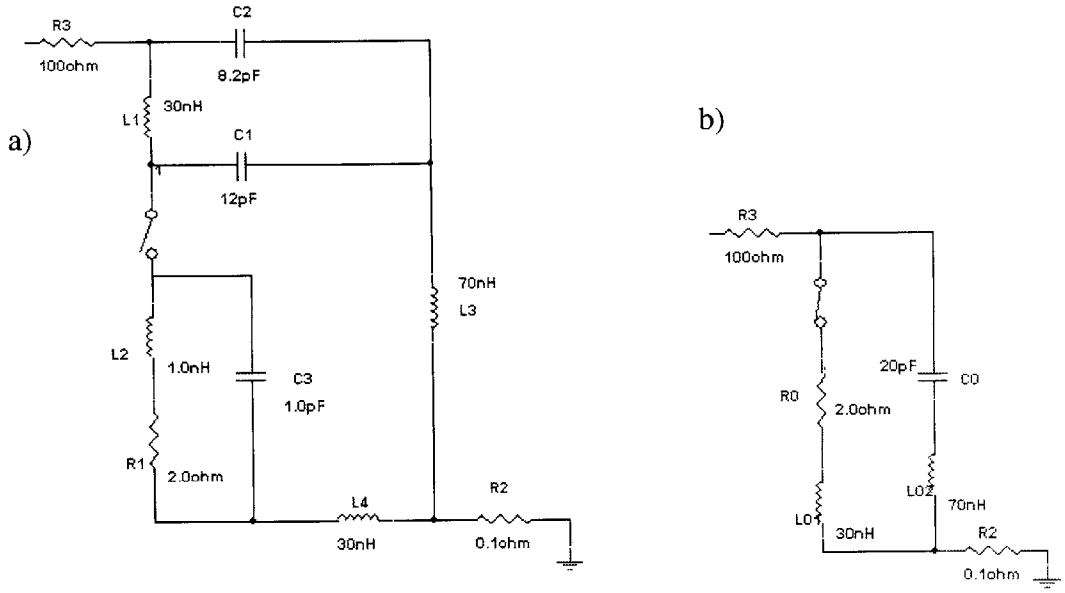

Figure 2-15 a & b Model circuits of the test gap

Component	Description	Method of Estimation	Value
R1	Arc Resistance	1,2,3	0.8-6.2 Ω
R2	Current Sensing Resistance	Known	0.1 Ω
R3	Added Series Resistance	Known	0-5000 Ω
C1	Plug Capacitance	Measured	12 pF
C2	Assembly Capacitance	Measured	8 pF
C3	Gap capacitance	Calculated	10^{-3} pF
L1	Plug Core Inductance	Calculated, 1,3	30 nH
L2	Arc Inductance	Calculated	<1 nH
L3	Assembly Inductance	Calculated, simulated, 1,3	70 nH
L4	Lower Ass'y Inductance	Calculated, simulated, 1,3	30 nH
R0	Arc Resistance	1,2,3	0.8-6.2 Ω
L01	Upper Inductance	1,3, simulation	70 nH
L02	Lower Inductance	1,3, simulation	30 nH
C0	Combined Capacitance	Measured	20 pF

Table 1

Parallel Capacitors

As has been seen in figure 2-9, adding external capacitors changes the ring frequency. Knowing that $\omega = \frac{1}{\sqrt{LC}}$ L can be approximately calculated from the observed ring frequency. Fortunately the decay of the ring is long enough that it can be measured. The decay also gives a value for R. The decay of an under damped system falls as a function of $e^{-\alpha\alpha}$ where $\alpha = \frac{R}{2L}$ it is easy to solve for R once L is known. The shots were all taken with 500Ω series resistance at 24kV. The results are in the table 2 below

Capacitance	Ring Frequency	Inductance	Resistance
104pf	50MHz	9.74E-08H	1.8 Ohms
104pf	50MHz	9.74E-08H	3 Ohms
104pf	50MHz	9.74E-08H	2.25 Ohms
240pf	30MHz	1.15E-07H	2.45 Ohms
240pf	30MHz	1.15E-07H	2.45 Ohms
240pf	30MHZ	1.15E-07H	2.28 Ohms
Average		**100nH**	**2.4 Ohms**

Table 2

Gap Voltage and Arc Resistance

Looking at the voltage plot in figure 2-12, it is clear that there is too much noise and the trace is too close to 0 to accurately gauge what the gap voltage is during breakdown. The probe has to deal with a 25kV pulse so it is not surprising that a signal as low as 100 volts is easily lost in the noise of the 1000x probe during a spark discharge. The low voltage can still be extracted from the data however with a little post processing. By applying a 5-point moving average to the signal much of the noise is eliminated and the low voltage signal can be seen more clearly. The data points are taken at 4ns intervals, so this moving average is really a 50MHz digital filter, rejecting all the high frequency noise. Using this method the gap voltage could be determined over the whole range of series resistance conditions except with 5KΩ where the breakdowns came too late for the capacitive ring to die sufficiently to get a good signal. As can be seen in table 3 below, the gap resistance increases as the series resistance increases. This is likely because the higher series resistance limits the current that flows and thus the size of the arc channel that is developed. If the cross section of any conductive medium decreases,

the resistance will increase. The different arc sizes can be noted by examining the size of the halos in the video images under different series resistances. Compare the halo in figure 2-13b with 100 ohms in series and the halo in figure 2-22a with 500 ohms.

External Series Resistance	Arc Voltage	Average Arc Resistance
0	380	0.8 Ω
100	290	1.8 Ω
500	190	4.4 Ω
1000	140	6.2 Ω

Table 3

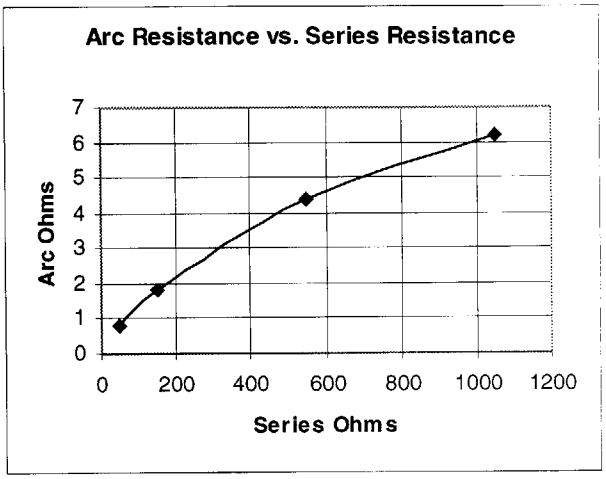

Figure 2-16 Arc resistance as a function of arc current →

From the data in table 3 a power-law model for the arc resistance as a function of arc current was derived:

$$R = 54i^{-2/3}$$

R is the arc resistance in ohms and i is the arc current in amps. This equation gives a very good fit to the measured values.

Determination of System Function

A final method to determine the component values of the test gap assembly was to extract the system function from the data. Since breakdowns occur so fast (typically in less than 2 data points) they can be approximated as a step function. The voltage across the current sensing resistor can then be taken as the step response of the system. The step response is helpful because its integral is the impulse response, and the impulse response of a system can completely describe that system. To get the impulse response, the derivative was taken digitally by $h[n] = s[n] - s[n-1]$. Then a fast Fourier Transform was applied to the impulse response to give the frequency response of the system. A Bode plot was made from the frequency response for comparison against the bode plot of the model. The bode plots of actual shots are very similar to the bode plot of the system

estimated with the previous two techniques [Fig. 2-17], thus confirming their accuracy. With higher bandwidth scope data this technique could be use to more precisely locate the poles and zeros of the system and solve for component values directly. However, the system resonance is right at the edge of the scope bandwidth in multi-channel mode, and so does not give reliable results for solving for the poles and zeros.

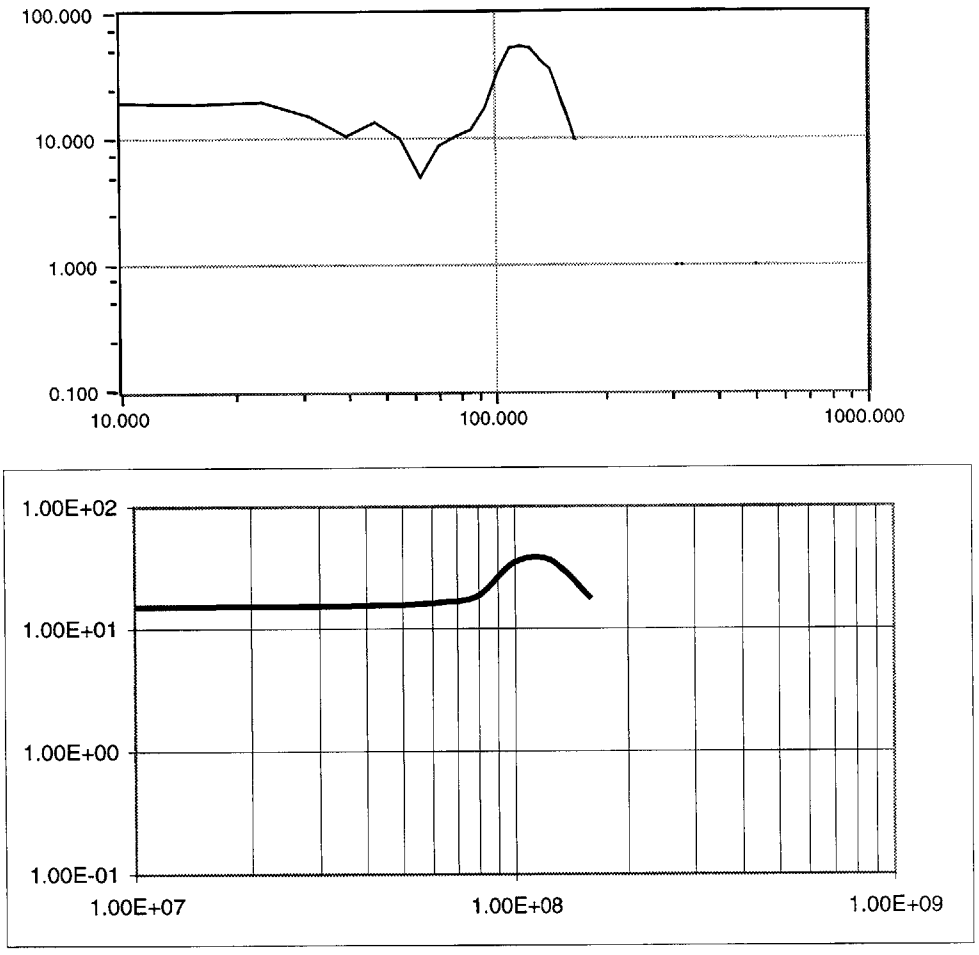

Figure 2-17 Typical Measured (top) vs. simulated (bottom) system bode plot.

The parameters for the simplified model circuit of figure 2-15b were put into a P-SPICE simulation of the test gap assembly. Figure 2-18 shows output plots of that simulation. Comparing the plots to figure 2-12 they are very similar, demonstrating the strength of the model, but there are a few notable differences due to limitations of both the scope and simulator. The current tail seen in the real data does not appear in the

simulation. This is because the voltage pulser is simulated by a simple square wave voltage source. As it will be seen in the next chapter, the NDBD pulser has a tail due to high frequency losses in the pulser itself. The probe used to measure the voltage had a bandwidth limit of 75MHz, and so the 105MHz ring visible in the simulation is not visible in the real voltage data. The scope was also only sampling at 125MHz, so the current trace may also suffer from some aliasing. The shot #060400.25kv.100.NGK.013 was chosen for figure 2-12 because it appears that the ring frequency coincided with the scope's sampling well and hence yielded clear oscillations. Other shots did not always have such a clear waveform.

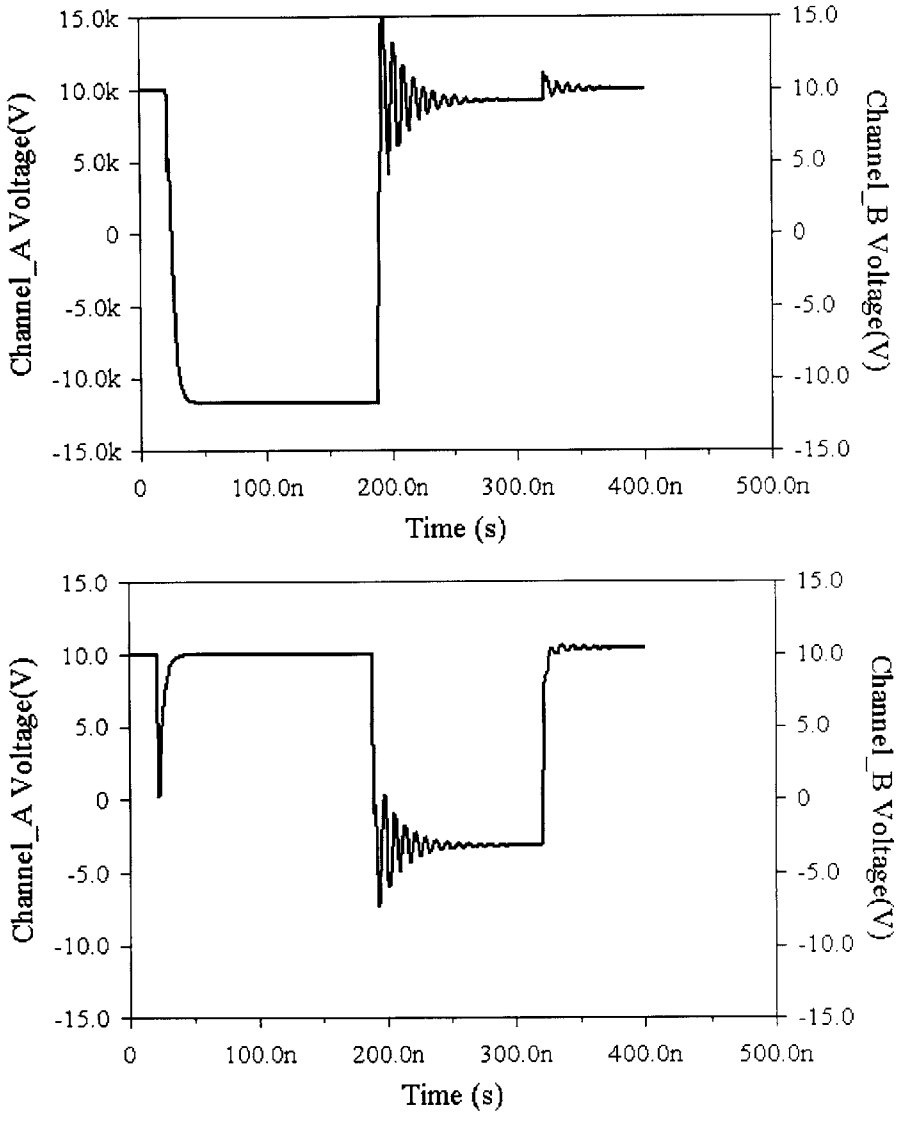

Figure 2-18 Voltage (top) and Current (bottom) of simulated test gap. Compare to figure 2-12

2.2.4 Gas Release

Another measure of the effect on the oil due to breakdown is the volume of the gas that is released by the spark. There seems to be some debate over the exact circumstances that form bubbles [7,8,9,10] when there is a liquid breakdown, but whatever the mechanism, they represent a possible change to the oil, and hence were selected to be minimized. Two characteristics of gas release were observed in the video images: the size of bubbles, and their motion. The electric drive circuit and components were purposefully altered to change the discharge currents and energies so as to reveal a broader range of test results

Although the gas measurements are based on observations of bubbles, the word "bubbles" may be misleading as to their nature. The "bubbles" may not result from classical mechanisms such as boiling or gas flow, but may instead result from processes like cavitation and represent temporary microscopic voids. For lack of a better word, these tiny spheroid regions will be called "bubbles".

2.2.4.1 Gas Volume

The volume of gas released was estimated by examining the video images frame by frame. The frame speed was standard 30 frames per second NTSC video. Measurements were based on bubble size. However, this was a rather difficult process due to several factors. To be accurately measured, the bubbles not only had to stay in the camera's field of view, but they had to remain in the camera's focal plane as well. The countable bubbles also could not have broken apart into many smaller bubbles too obscure to quantify. Events were selected to satisfy good visualization. However, 12 clear and unambiguous shots were obtained. [Appendix D] These 12 shots were enough to build a strong correlation between the measured currents and the size of the bubbles. Typical observed sizes ranged from 50μm to 1200μm in diameter.

The following model was developed for the volume of observable gas resulting from discharge events. The model is physically based and is simply that the volume of gas observed after a test event is proportional to the electrical energy dissipated in the oil. Figure 2-19 shows the nice linear relation between the measured gas volume as a function

of the measured $R\int i^2 dt$ (joules). The resistance R is the arc resistance as determined in section 2.3, the current i is measured by the 0.1 ohm resistor connecting the return ground side of the gap to the system ground. The energy value assumes the discharge resistance is reasonably constant for the duration of the breakdown. The experimentally derived formula for bubble volume is:

$$v = .013R\int i^2 dt$$

where v is the bubble volume in mL and i is the measured current in amperes. $R\int i^2 dt$ is more accurately quantified than $V\int i dt$ because it does not involve extracting the gap voltage for each shot. The gap voltage can be averaged out to approximate R, but it is not nearly as clear a signal as i, and so was not used to find the energy on a shot by shot basis.

The fact that bubble volume is not a linear function of $\int i\ dt$ or $R\int i\ dt$ [fig 2-20] indicates that the bubble size is not so dependent on the amount of charge that is dumped into the gap or the voltage across the gap, but rather on the total energy which is dissipated in the gap. Typical discharge energies were on the order of 100 μJoules with a charge transfer of 10 μCoulombs and released gas on the order of 10 nano-Liters. One reference for comparison [14] provides results that indicate micro-discharges in transformer oil release as much as 1μMol per μJoule of energy. The volume produced in the NDBD tests was about 30 times less.

To confirm that the bubble volume was indeed a function of the total current and not just the peak current, a special ground side impedance was added to cut off current in the gap as soon as it started. This was accomplished by a series circuit of a 125pf capacitor in parallel with a 2MΩ resistor. [Fig 2-21] The capacitance charged up during a breakdown so as to raise the voltage on the ground electrode up and reduce the voltage across the gap. By lessening the voltage across the test gap after breakdown less current would flow through the oil, leading to reduced effects to the oil and electrodes. The 2MΩ resistance on the ground side drains the capacitors so the ground side of the test gap will

be 0 before the next shot. The 2MΩ is large compared to the resistance of the gap during breakdown and hence does not influence the breakdown.

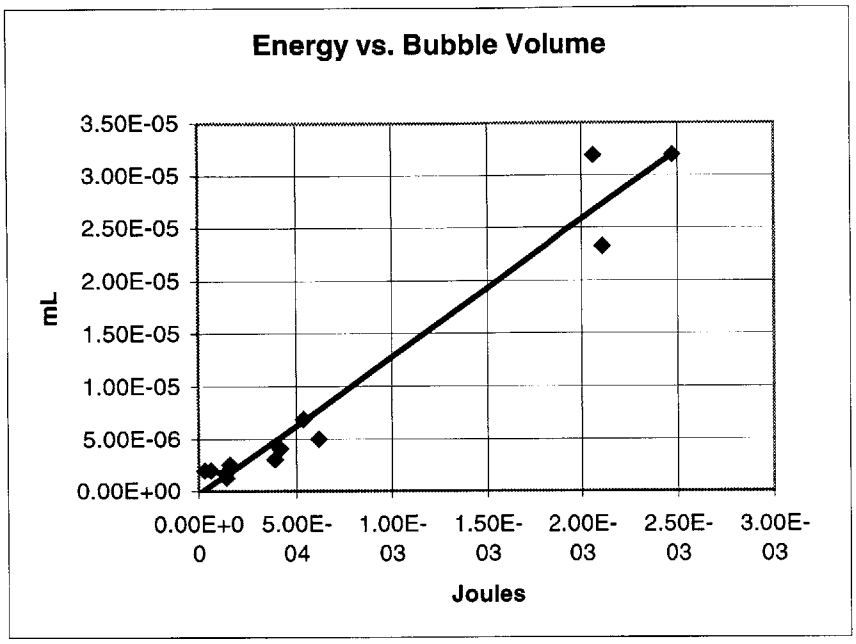

Figure 2-19 Bubble volume as a function of energy

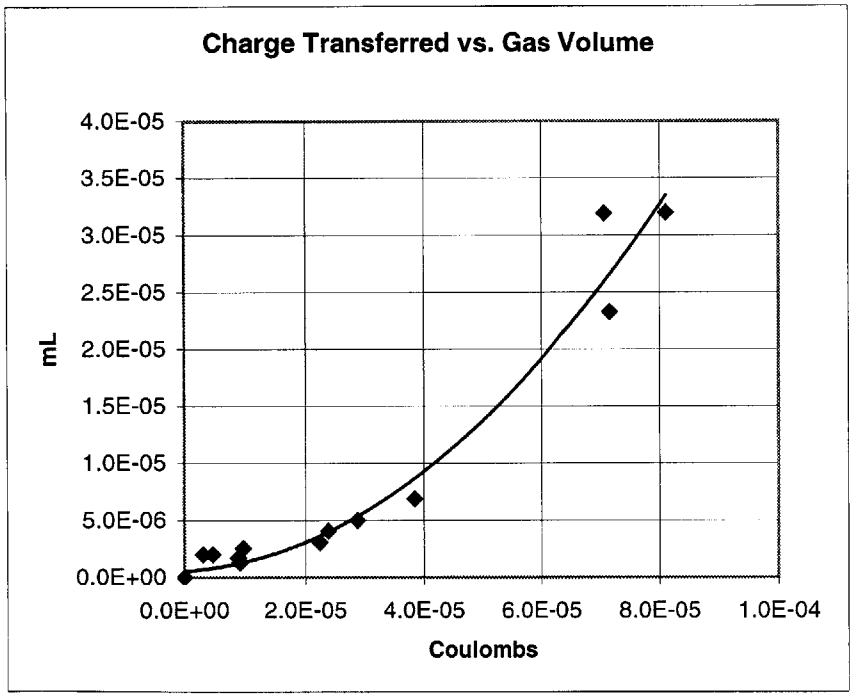

Figure 2-20 Bubble volume vs. Coulombs of charge transferred. Including displacement current. A small $<10^{-6}$ C amount of charge used to charge the gap capacitance could not accurately be removed from the measurements

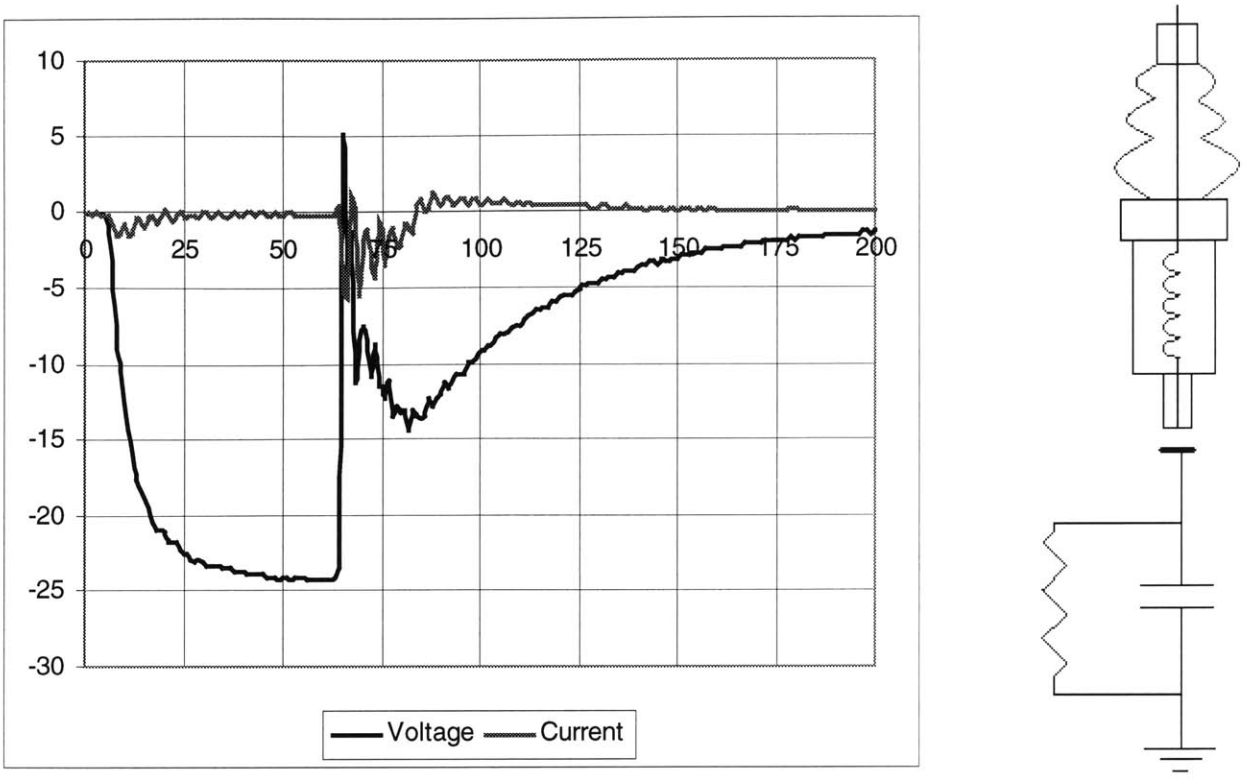

Figure 2-21 Measured voltage and current with capacitive impedance, and diagram of capacitive ground impedance. Compare to voltage and current waveforms of figure 2-12

As can be seen in table 4 the volume of gas released was greatly reduced with the addition of the ground side impedance, confirming the effect of steady current on bubble volume. Unfortunately the precision 0.1Ω resistor for current measurement could not safely be placed right after the gap, but instead was placed between the impedance and ground. The $\int i^2 dt$ from the resistor looking through the capacitors is not likely to be an accurate a measure of the current flowing through the gap itself. While the total charge transferred will be the same, i^2 will not.

Conditions	Average Gas volume
500Ω in series, 24kV, direct gnd. connection	7.6E-06 mL
500Ω in series, 24kV, capacitive gnd. impedance	2.0E-06 mL

Table 4

2.2.5 Oil Motion

By far the most interesting and unexpected phenomenon in the oil gap breakdown is the motion of bubbles seen in the oil; namely a rapid radial velocity away from the gap. While the ejection distance did grow with the gas volume, closer inspection of the data revealed that the motion was not governed by the same model as the gas volume. By examining the different ejection distances within the different test conditions it became clear that the bubble ejection distance was most closely correlated to the peak transient current of the breakdown. [Fig 2-23] Still, a completely clear and definitive model of the bubble ejection phenomenon could not be developed from the observed data. However, the following observations seemed very reproducible:

1) Bubble ejection distance is highly correlated to the peak transient current. [Fig 2-23] The time to breakdown, and $R\int i^2 dt$ are not as highly correlated
2) The direction of ejection is consistently in the same direction of any bow in the arc [Fig. 2-22a-b]
3) Bubbles are most often ejected as a single large bubble [Fig. 2-22c]
4) The bubbles are either carried out by a fluid flow, or create a visible fluid flow with their motion [appendix C] [Fig. 2-26]
5) Within a group of bubbles, the smaller bubbles will be carried/ejected as far or farther horizontally than the larger ones in the same event [Fig. 2-22e, 2-22c note small bubbles]
6) When there is a no breakdown event, motion in the fluid has still been observed and appears to follow a symmetrical pattern down the point and radailly along the plane [Fig 2-26]

2.2.5.1 Oil Motion Models

The potential causes for the oil motion in these results are considered further in the following five different models: rail gun, thermal expansion, electric field, ion drag, and peak current.

a)

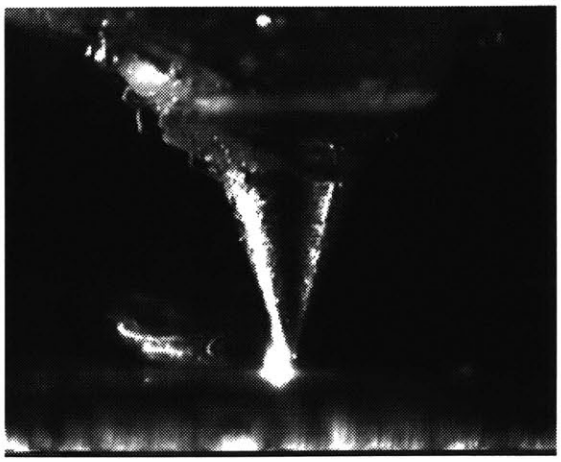

b)

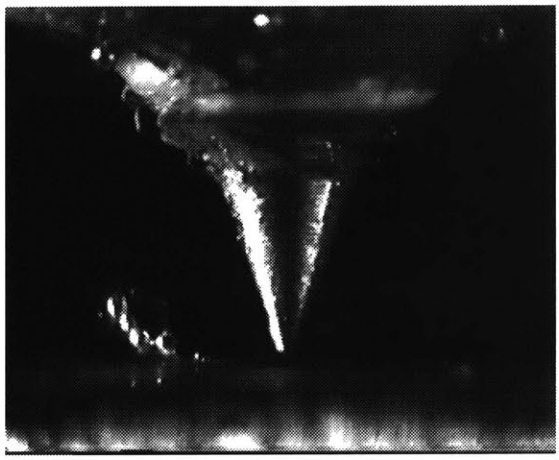

c)

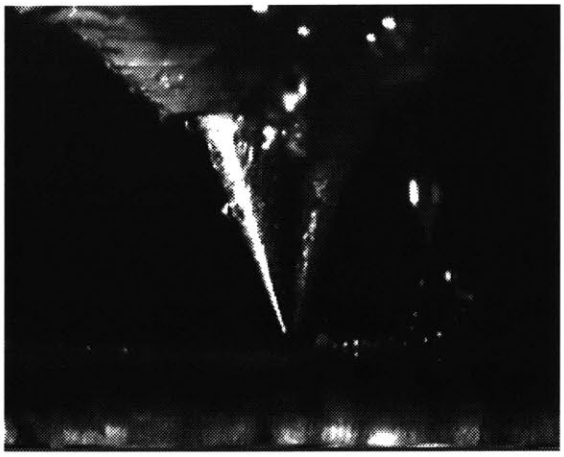

d)

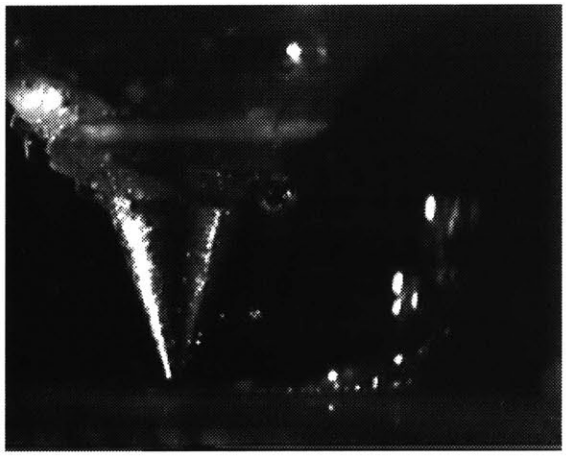

e)

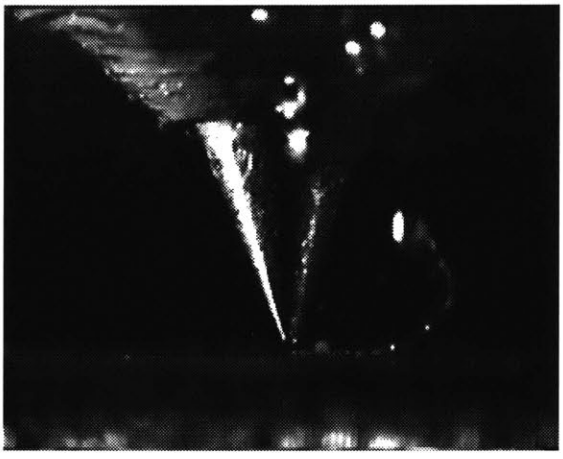

Figure 2-22

a), b) showing ejection of bubbles in the direction of arc bowing

c) singular bubble

d) fragmented bubbles

e) tail of many tiny bubbles

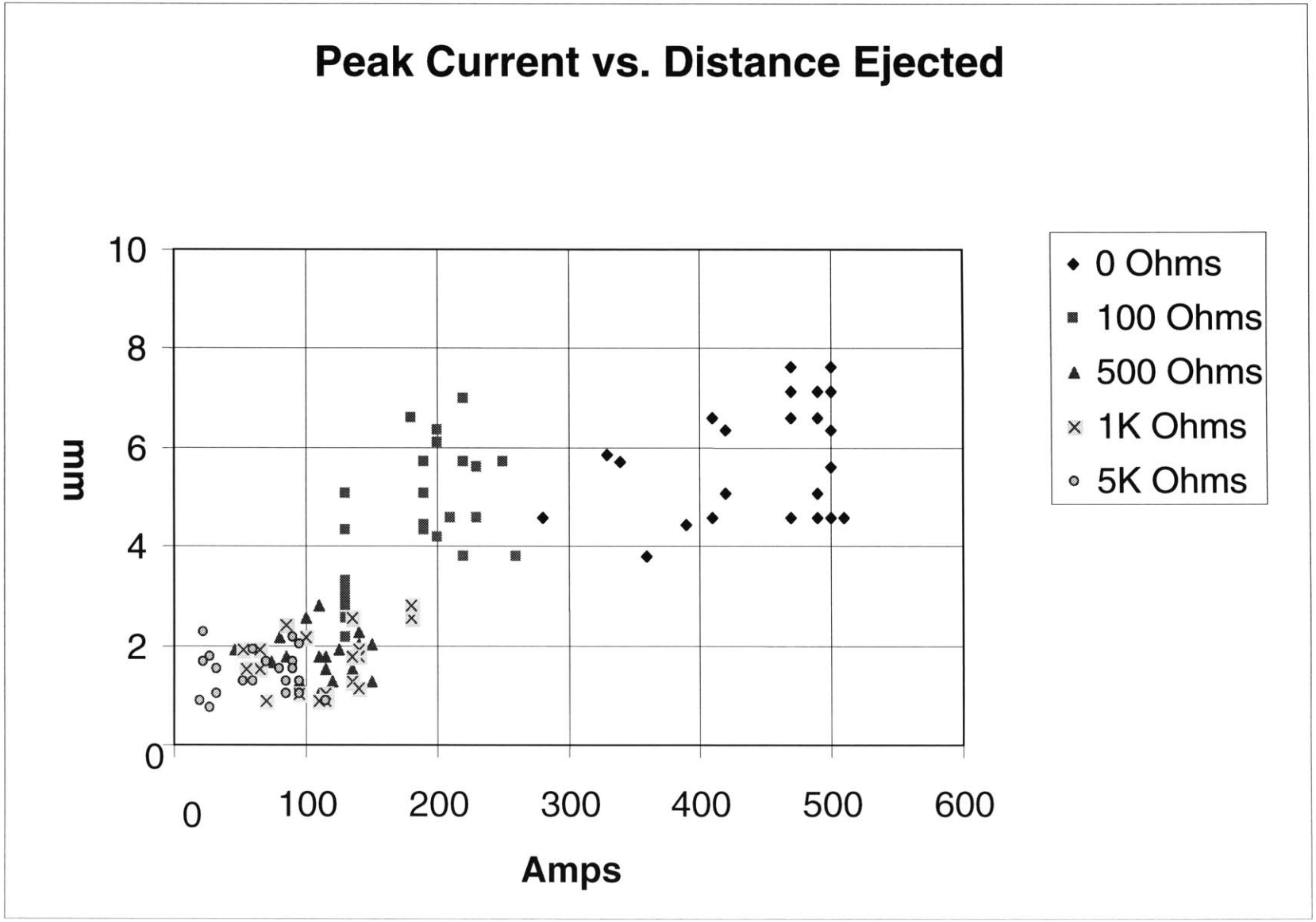
Peak Current vs. Distance Ejected
10
8
6
4
2
0
mm
0
100
200
300
400
500
600
Amps
0 Ohms
100 Ohms
500 Ohms
1K Ohms
5K Ohms

Figure 2-23

Current (Rail Gun) Ejection Model

The consistent ejection of the bubbles in the direction of arc bowing would seem to indicate some sort of radial force such as a current loop expansion force ejecting the bubbles. As in a rail gun the current flowing through the loop forces the bubble (or rail gun slug) outwards. [Fig 2-24] The rail gun model could provide a mechanism for the fluid flow as well. As the bubble is ejected it must push some oil out of the way and due to viscosity, drag some oil with it. The oil moved by the bubble will create a radial flow in the direction of ejection, which would help explain the movement of smaller debris along with the main bubble. The rail gun model would certainly seem to have the necessary energy to create such a violent bubble ejection and oil flow. The resistance force on a spherical surface traveling through fluid increases to the square of the velocity [11]. Thus, if the bubble were being ejected with a force that is increasing linearly with current, its ejection distance would be an inverse square function of the ejection force. So if the peak current is creating an impulse force on the bubble, the distance will be an inverse square function of the peak current. The graph of ejection distances can be easily fit by an inverse square function.

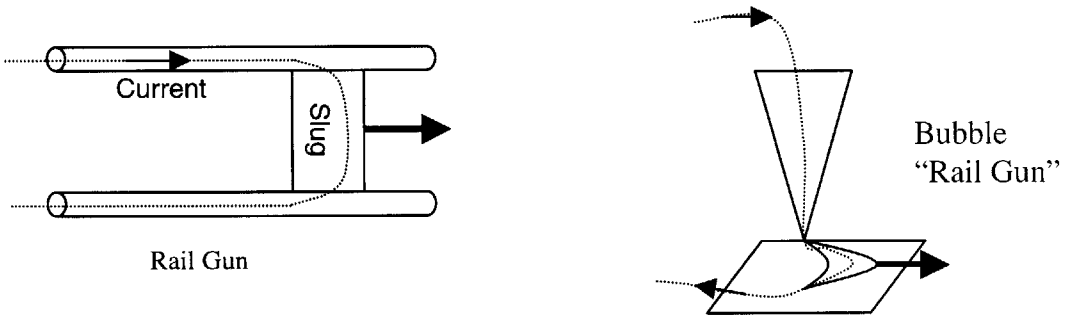

Figure 2-24 Rail Gun Model for Bubble Ejection

While the rail gun model may seem very plausible, it does not fit some of the observations. The force on the rail gun slug and therefore its' velocity is proportional to $\int i^2 dt$ [12], yet the bubble ejection distance is mostly peak current dependent and not well related to $\int i^2 dt$. Another inconsistency is that the ejected bubble is usually a single whole bubble. It would seem that if the electric forces were launching the bubble outwards it would tear into smaller pieces as the arc deforms outwards. Finally, the oil

flow would be entirely along with the bubble's motion and not form the observed symmetrical circulation.

Thermal Expansion

Another mechanism for the ejection of the bubbles is the rapidly expanding hot gas formed during the arc being forced out from underneath the needle point. The arcs usually form near the edge of the needle where due to a slight oblateness of the particular plug tip the curvature is still the greatest. This location would cause a bubble to be formed partially under the needle point and partially out in the open. As the bubble expands it will extend outwards from underneath the point rather than contracting under to a more confined space. This expansion of the bubble out from under the needle could account for the bowing of the arc outwards since the arc is traveling through the bubble. However, it seems unlikely that the bubble would extend out so violently to account for its' speed and the flow in the oil. Additionally, there is no reason for the bubble to stay in the horizontal plane. The path to greatest expansion for the bubble is not hugging the bottom plane, but rather slightly upwards, expanding between the plane and the side of the needle.

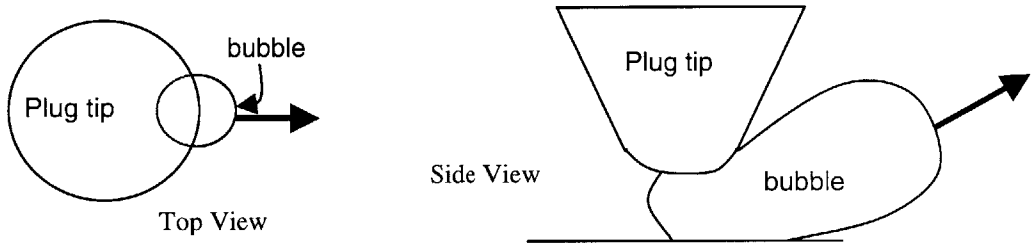

Figure 2-25 Thermal Expansion Model of Bubble Dynamics

Voltage Dependence

It may be possible that the bubble ejection distance is a function of the gap voltage. However this theory seems very unlikely because the voltage across the gap is nearly always at the maximum 20 or 24kv prior to breakdowns Furthermore in contradiction to a voltage dependence bubbles were ejected the full spectrum of distances with the same gap voltage.

Ionic Drag/Wind

The key observation that cannot be explained by any other model is the motion of fluid as detected by debris near the needle tip after the firing of a non-breakdown event. As the tip of the needle reaches voltage there are carriers, such as electrons, which can be driven toward the positive ground plate below. As they travel from the tip, these carriers collide with oil molecules forcing them to flow if caught in the friction of a wind along the observed flow pattern. [Fig 2-26] Unlike any of the bubble initiated flow patterns this "ionic wind" model can account for the fully symmetrical flow pattern sometimes seen. However it would be surprising if there were sufficient time for the "ionic wind" to build up enough speed to account for the rapid bubble ejections seen. In fact as stated before, the distance ejected is not affected by the time until breakdown – the time the ionic wind would be on to set up flow before a bubble forms. Fluid motion in the point to plane gap under non-breakdown conditions has already been documented by other researchers [13], however, any pre-breakdown current in the NDBD tests was to small to be measured, and there appears to be no theory as to what causes such a sudden flow just prior to a breakdown

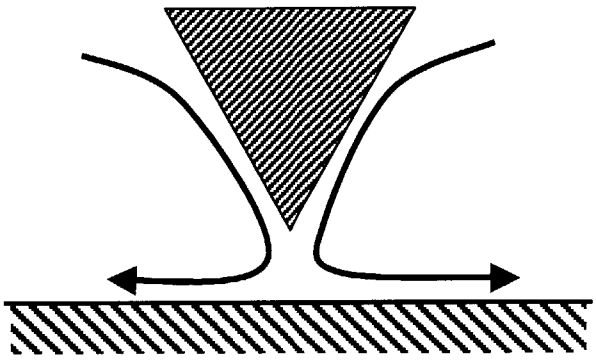

Figure 2-26 Diagram Illustrating Observed Oil Flow

Current Peak Initiated Flow

Because of the fact that strong symmetric circumferential flow patterns are observed in the motions of small bubbles [appendix C] and that small bubbles are sometimes carried farther than large ones, it seems that a symmetrical oil flow must somehow be heavily involved in the ejection of the bubbles. Since the bubbles are ejected

asymmetrically and the flow seems to be symmetric, it seems more likely that the oil flow is a cause rather than an effect. If the flow is generally radially outward along the bottom plate as observed, oil velocity will then decrease with the inverse of the radius. The bubble will also slow due to viscous drag forces, which act linearly in proportion to the velocity. [12] Thus the velocity $\frac{dr}{dt} \propto \frac{1}{r}$, and $\frac{d}{dt}\ln(r) = \frac{1}{r}$ so the plot of ejection distances vs. initial velocity will follow a logarithmic curve. The plot of ejection distance vs. peak current is well fit by a logarithmic curve suggesting the possibility that peak current could somehow induce an initial flow to the oil.

If bubble motion is indeed controlled by the oil motion, no reasonable model for oil motion in terms of peak current has been found. It may be that the measured transient peak is an indication of something else, or that the height of the step to the peak of that first transient current does indeed move the oil in some way, but there is of yet, no solid model for this phenomenon.

Model Evaluation

It is possible that bubble ejection is a combination of the models proposed. Perhaps the ionic drag forces set up a flow that along with the thermal expansion of the bubble creates a bow in the arc to initiate a rail gun effect. Perhaps the first and peak impulse of current creates some sort of flow that carries the bubbles outwards. What is clear is that some undiscovered process that controls the peak current also controls the bubble ejection distance. With very high speed video and higher bandwidth probes more details of the bubble and breakdown process could come to light. However, there is presently not enough information to build any solid theories. This phenomenon definitely warrants further study outside of this thesis. In terms of any effects on the oil, the mechanism that governs the bubble ejection seems to be separate from the mechanisms that control the volume of the bubbles For now, bubble ejection will be taken as a function of peak transient current powered by phenomenon that remains unclear.

2.3 Ideal Test Gap

Mechanically, spark plugs are a good choice for mounting on a transformer. Electrically, however, the plugs will have to be modified or custom manufactured. Though a point to plane gap can be crudely machined with some off the shelf plugs [Fig 2-27] there remains some electrical characteristics that must be dealt with. An ideal plug would have very low capacitance to minimize the energy that must be pumped into the gap to bring it up to voltage. A lower capacitance plug can use a higher series resistance on the input for the same *RC* time constant. While some current ringing does not contribute significantly to effects in the oil, extensive ringing can lead to an increase in $\int i^2 dt$. To prevent this the inductance of the plug should be kept to a minimum by using a thick core, and it should have an internal resistor to damp the oscillations

Figure 2-27 Off the shelf plug machined to a crude point to plane

2.3.1 Close Coupled Resistance

One way to block the effects of the stray inductance and capacitance from the gap is to place the series resistance as close to the tip of the plug as possible. Resistive spark plugs are built with an internal resistance that could accomplish this. Resistive spark plugs have many of the desired features for an oil test gap. Unfortunately they are designed around automotive parameters and need to be modified in order to work well in an oil test environment. Automakers added an internal resistor to the plugs to reduce fast pulse current that radiated pulse energy and interfered with the car's radio reception. The resistor values were chosen for the near milli-second discharges of an automotive spark plug, not the desired 20nS rise time of the NDBD pulse. Typical resistive plugs have a resistance of 5KΩ, which combined with a typical capacitance of 10 pf, leads to a time constant of 50ns, unacceptable for the NDBD pulse. [Fig 2-28] 500Ω –1000Ω seems to be the maximum series resistance that does not affect test performance with a 10pf plug. An ideal custom resistive plug would then have a very small capacitance, maybe 5pf, and an internal resistance of 1000 Ohms. In the AC R45TS resistive plugs that were dissected, the resistor element penetrated nearly to the very tip

of the plug. This feature is very desirable in a custom plug as it blocks some of the jacket capacitance from the gap.

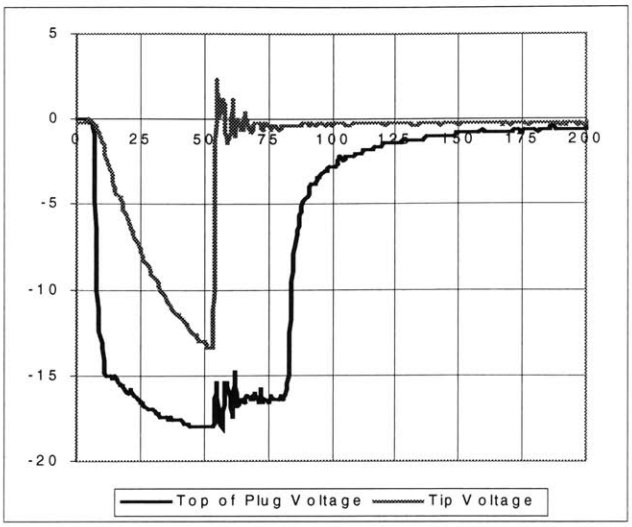

Figure 2-28 Voltage at tip and terminal of resistive plug. Gap was closed to .004" to enable breakdown at lower tip voltages. Note the slow rise of the tip voltage

2.3.2 Recommended Test Gap Design

Taking into account what was learned about gas ejection and oil motion, the ideal NDBD test setup would consist of the custom plug of section outlined in 2.3.1 above, with the capacitive current limiting impedance of section 2.4.1 on the ground return. This arrangement would limit the amount of transients and also block any current flow after breakdown, keeping gas volume to a minimum. As reducing the plug capacitance may not be possible, an alternative is floating the jacket of the plug. This method was used in an early version of the test for convenience, but when examined, has some clear value in reducing the capacitive energy dumped into the gap. [Table. 5]

Conditions	Measured C	Average $\int i^2 dt$	Average Gas Volume
Plug Grounded	20 pF	4.7×10^{-5} J^2S	7.5×10^{-6} mL
Plug Floating	10 pF	4.3×10^{-5} J^2S	2.0×10^{-6} mL

Table 5

An idealized setup using non-custom plugs is outlined in the diagram below.

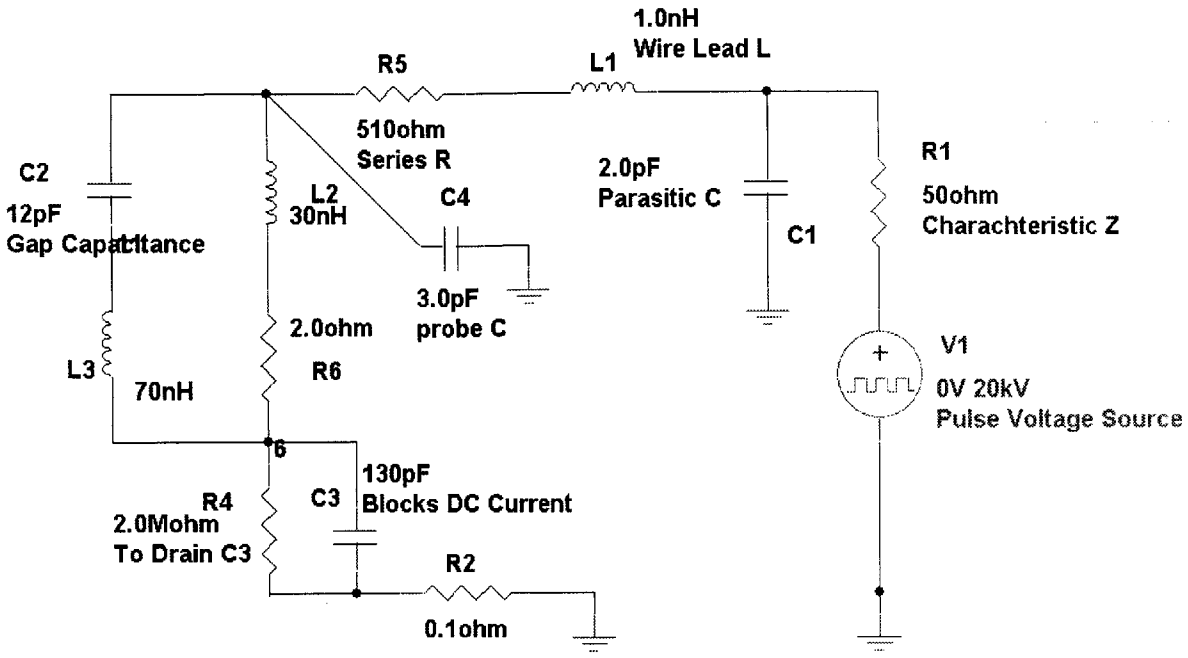

Figure 2-29 Circuit Diagram of 1999 Pulser Setup

The floating plug test arrangement circuit was put into the P-Spice simulator to verify the model of all the sub-circuits developed and confirm what happens with the use of the capacitive impedance on the ground path. The real and simulated waveforms are below:

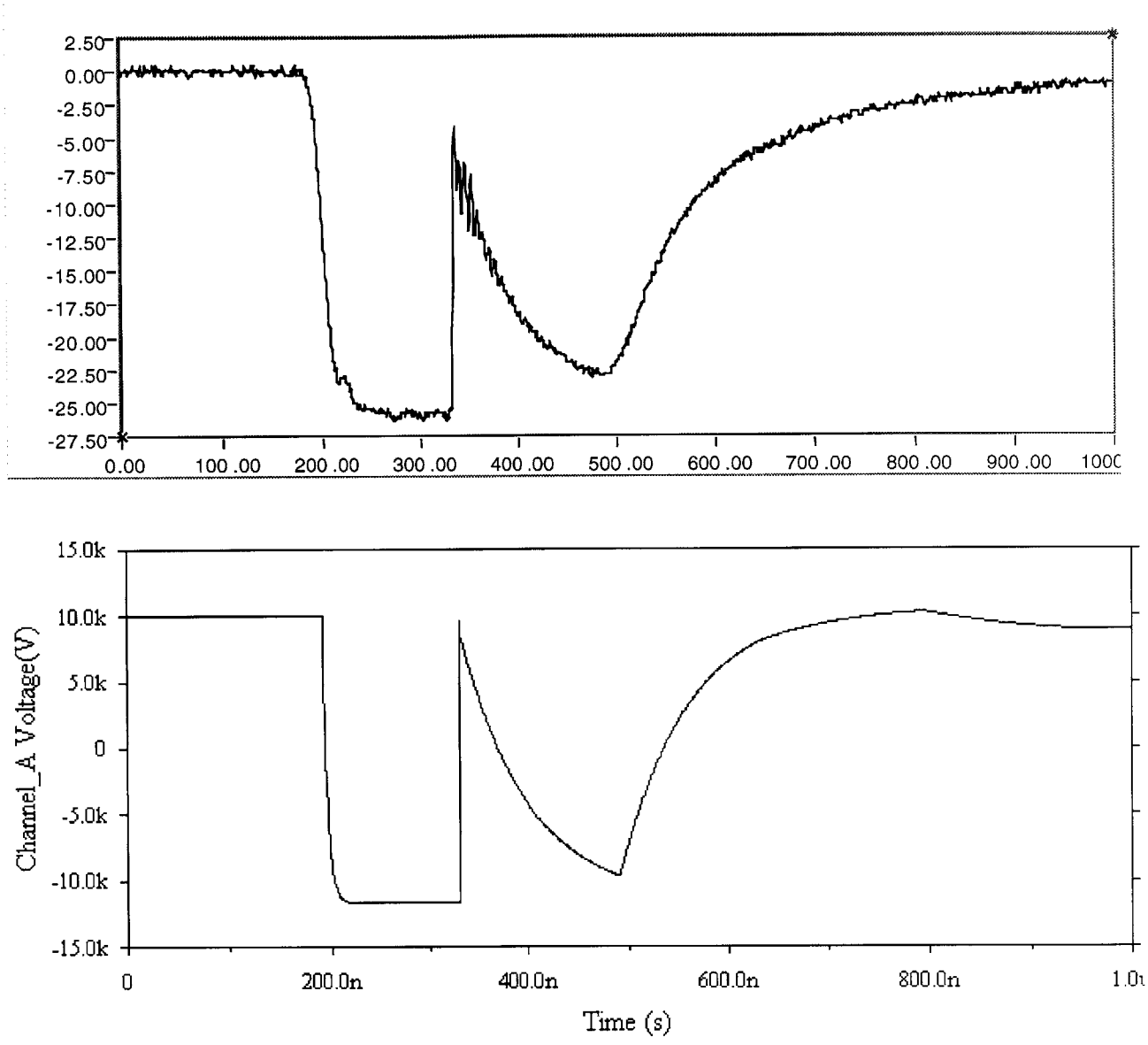

Figure 2-30 Measured waveform (top) and simulated (bottom). Also compare to figure 2-16

To minimize effects in the oil, the design parameters for using an off the shelf plug and custom plug are outlined as follows:

Off the Shelf Plug

A non-resistive plug such as the NGK BP6ET is machined to a point and screwed into an insulating plate. A brass plate is mounted underneath the point and tied to the ground return with the 125pf impedance. The "On" current is limited by this impedance and a 1KΩ series resistance on the input. The design method for such a test gap is simply:

1) Minimize the gap and plug capacitance as much as possible through mechanical means. This will enable maximizing the series resistance, reducing "on" current
2) Add a series input resistance such that RC = 10ns
3) Add a 125pf capacitance in series with the ground plate to block any follow-on current
4) Machine tip to cone angle of 30° if possible
5) Break in plug until tip radius reaches 100μm, then reset gap

Custom Designed Plug

Custom manufactured plugs offer several advantages including better preparation of the point to plane gap. The gap can be set as part of the manufacturing process and coated with erosion resistant materials instead of being turned down from a stock plug by hand. The custom plug should be designed with the following parameters in mind:

1) Above all else, minimize plug capacitance
2) Add an internal series resistance as close to the actual tip as possible to block as much capacitance from the gap as possible
3) The series resistance should be calculated from the capacitance visible to the gap where R=10ns/C
4) Make a cone angle of 30°
5) Form a tip radius of about 100μm

The non-custom version of this high reliability test gap configuration had already been arrived at by simple bubble observation in the earlier NDBD apparatus used to test

many of the oils. The exact reasons that arrangement is optimal were not entirely clear at the time, but now with a gas volume model and greater understanding of the physics involved in the NDBD breakdown, a better test gap based on a custom spark plug can be readily designed.

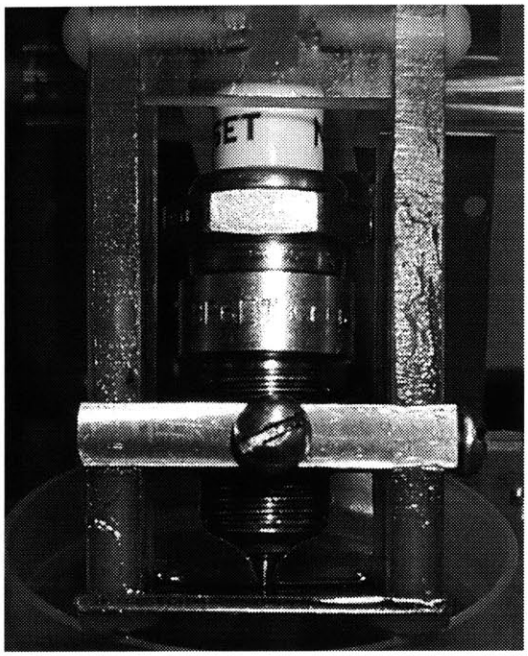

Figure 2-31 Test Gap Assembly used on 1999 Pulser

Chapter 3

Electronics

To be acceptable for placement on a live transformer, the pulser must limit the energy it can release if it should malfunction. Because of its inherent current limiting ability and its clean pulse, the transmission line type pulser was used in the original NDBD apparatus and has been compacted for use in the newer versions.

3.1 Transmission Line Pulser

The basic transmission line pulser employs a long coaxial cable with its length determined by the desired pulse width. One end of the cable is connected to the output. [Fig. 3-1] The operation of this pulser is rather clever as there are no components except the transmission line that the output must pass through, and there can never be any more pulse than the transmission line contains. Thus the quality of the pulse is limited only by the quality of the transmission line. Before a pulse is initiated, the shield of the cable is pre-charged to a DC voltage $+V_{chg}$ and the core remains at ground potential. To initiate the pulse, the shield is suddenly switched to

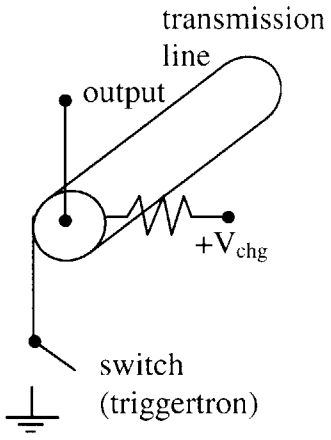

Figure 3-1 Pictorial Schematic of Pulser

ground with a spark gap switch. Because the voltage differential across the cable can only disappear as fast as propagation through the cable will allow, the voltage on the core switches from ground to $-V_{chg}$ when the voltage on the shield is switched from $+V_{chg}$ to ground. The voltage $-V_{chg}$ then begins to propagate along the length of the cable. The propagation speed and length of cable determine the width of the pulse. The RG-223 cable used in both the new and old pulsers had a propagation speed of 5ns per meter, so 60 meters were necessary for a 300ns pulse. Because the output signal is traveling through the cable, it is limited by the characteristics of the cable, namely the pulser has an output impedance equal to the impedance of the cable. The equivalent circuit of the output is shown in figure 3-2. A typical output pulse is shown in figure 3-3.

3.1.3 Pulser Characterization

The Thevenin equivalent model used for the pulser in figure 3-2 is a pulse voltage source in series with a 50Ω resistor. This model is adequate enough for NDBD simulation

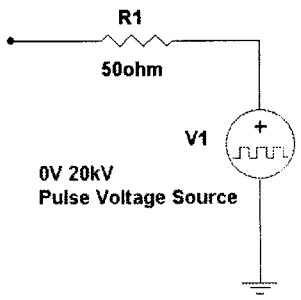

Figure 3-2 Thevenin Equivalent of Pulser

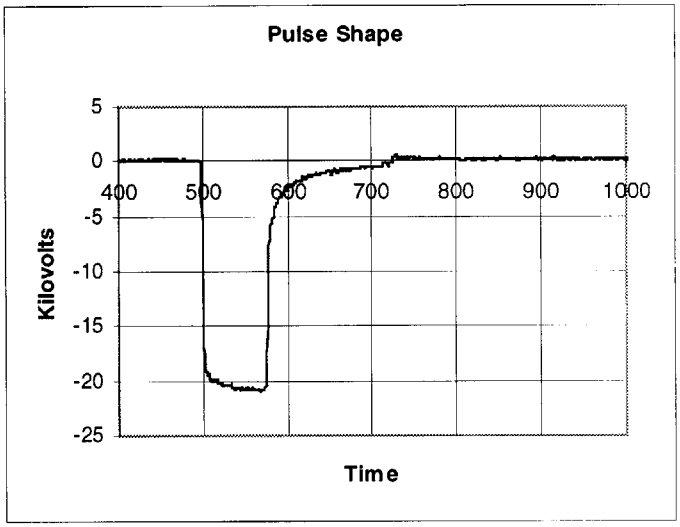

Figure 3-3 Unloaded Output of Pulser. Note tail on pulse due to skin-effect losses of high frequencies

purposes, but under careful scrutiny of the output pulse it is not entirely accurate. Before performing any tests evaluating effects on the oil, the exact characteristics of the pulser had to be defined. It was noted that the pulse rise time of 20ns was much longer than that of pulsers of similar design.

Characterization began with measuring the short circuit current. The short circuit current was very consistent with the Thevenin model using 50Ω. At 20Kv, the short circuit was a steady 400 amps except when it was less during the first 20ns due to the voltage still rising. The pulser was loaded with capacitors to see their impact on the rise time. Interestingly they had no impact until about 100pf was added, indicating that there was already an effective capacitance on the output of about 200pf. This capacitance seemed rather large to just be attributable to the internal geometry of the wiring. Another important fact was that this internal capacitance did not manifest itself in the short circuit current. If there were a large capacitance there would be a large current spike as it emptied during a short circuit or breakdown occurring after charge up. There was no such spike. A distributed inductance and capacitance model was developed to give the appropriate slow rise time, but as can be seen in figure 3-4, the distributed impedance did not show itself after charge-up because the voltage transition back to zero upon breakdown was essentially instantaneous. A final observation was that the rise time was not this slow with the previous pulser using an identical coil of transmission line but with the triggertron not located in the center.

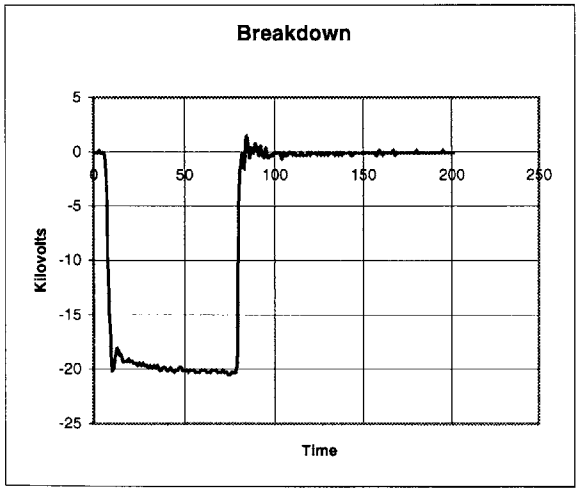

Figure 3-4 Plot of Measured Voltage of a Breakdown Shot. Note how fast breakdown occurs

The theory for the slowed rise-time in the new pulser is based on the fact that the triggertron is inside the coil of cable. [Compare figs. 3-6 and 3-9] In an effort to save space, the 1999 and 2000 versions of the pulser placed the triggertron inside the coiled up length of cable. The RG-223 cable has as insulating jacket over the shield, so when the ends of the shield are pulled to ground the signal does not propagate instantaneously through the coil. The signal must spiral around and around until it reaches the ground signal from the other side in the middle. It is thought that this spiraling on the first inside layer induces currents in the triggertron and connecting wiring inside the core. The time to circle the first layer would be about 15ns and could explain the slow 20ns rise time.

As can be seen in Figure 3-3, the pulse also has a tail. This is a result of the high frequency limitations of the RG-223 cable. Skin-effect losses attenuate the high frequencies as they propagate through the cable, leaving no high frequency components to create a sharp edge at the end of the pulse. This is of little concern to the NDBD test however, because breakdowns occur on the tail only extremely rarely.

The slow rise time was not perused at length for this thesis because whatever mechanism was causing it did not manifest itself after the first 20 ns. Since breakdowns do not typically occur in the first 20 ns, and about that much time is used to charge the test gap capacitance, this rise is acceptable. It would be interesting to explore the mechanism that is slowing the rise time, however it is not critical to the NDBD test and has the advantage to prevent inductive overshoot in the test voltage waveform.

It is concluded that that 50Ω resistive Thevenin model accurately portrays the pulse source that drives the NDBD test. This model is used in all of the NDBD circuit simulations presented so far, figure 2-18 and figure 2-29

3.1.1 Triggertron Switch

The original pulser for the NDBD system was quite large and bulky. [Fig. 3-6] The system had an external Glassman HighVoltage supply to provide the 25-35 Kv for its

operating range, and an external automotive capacitive discharge ignition system to trigger the pulser.

Triggering of the output was accomplished by a triggertron high voltage spark gap switch. The triggertron is a three-port device and consists of a pair of rounded electrodes separated by a gap of about 1 cm. There is a hole in the center of one of the electrodes, which has the pin of a small spark plug peeking up through it. [Fig 3-5] When the two electrodes are at their charged potential there is not enough voltage to cause a breakdown between the them. To trigger the device (to switch it on) a spark is created between the spark plug pin and the surrounding electrode by the triggering circuit. This spark releases ions into the space between the electrodes, triggering a breakdown between the two rounded electrodes activating the switch closure.

In the 1999 version of the pulser, the triggertron was moved inside the coil of coaxial cable to save space. The power supply and ignition module from the original system were used, but still the size difference is still quite large. [Fig. 3-7] The exact placement and arrangement of the triggertron evolved through 6 different variations before arriving at the present cross-arm version. [Fig. 3-8, 3-9]

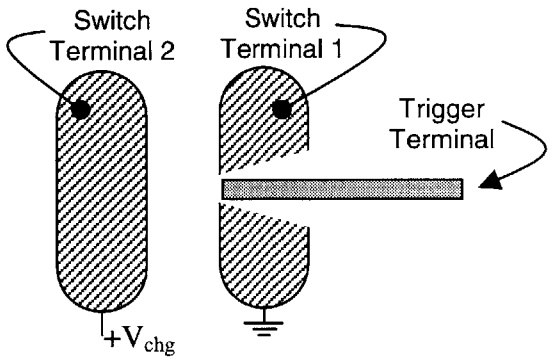

Figure 3-5 Basic Triggertron

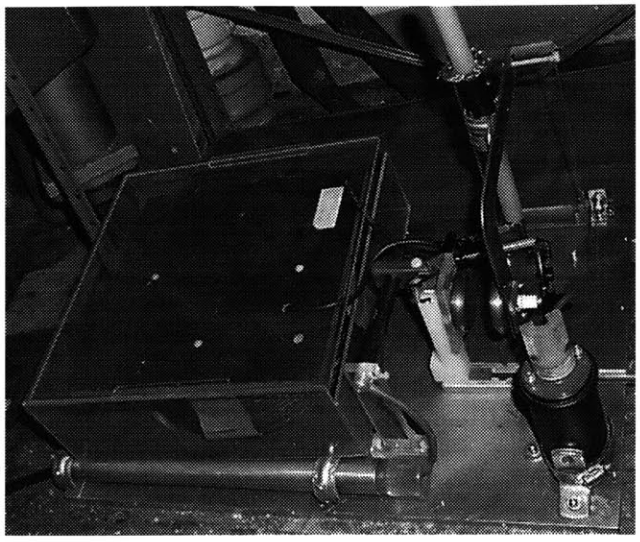

Figure 3-6 Early Pulser System with Cover Removed

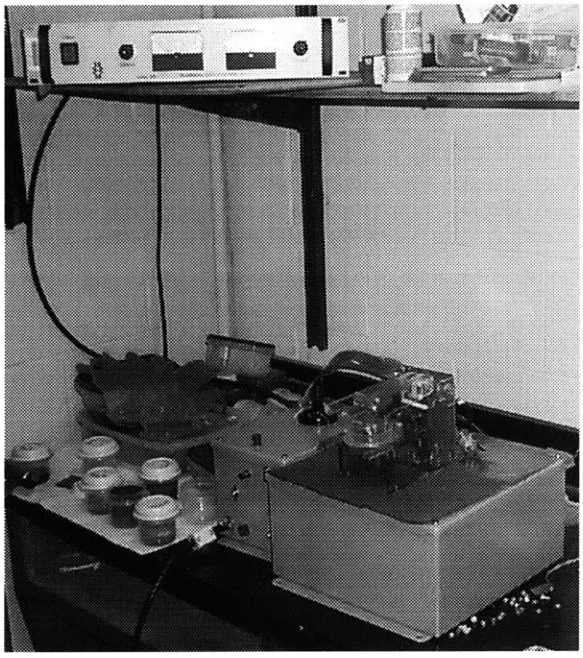

Figure 3-7 1999 Pulser Showing Power Supply on Shelf

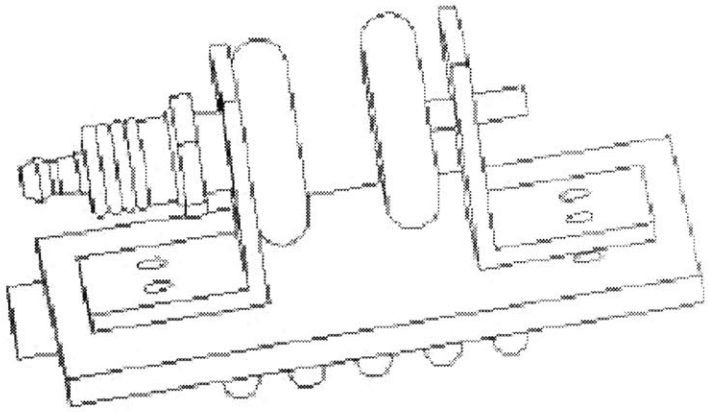

Figure 3-8 1st Triggertron design for New Pulser

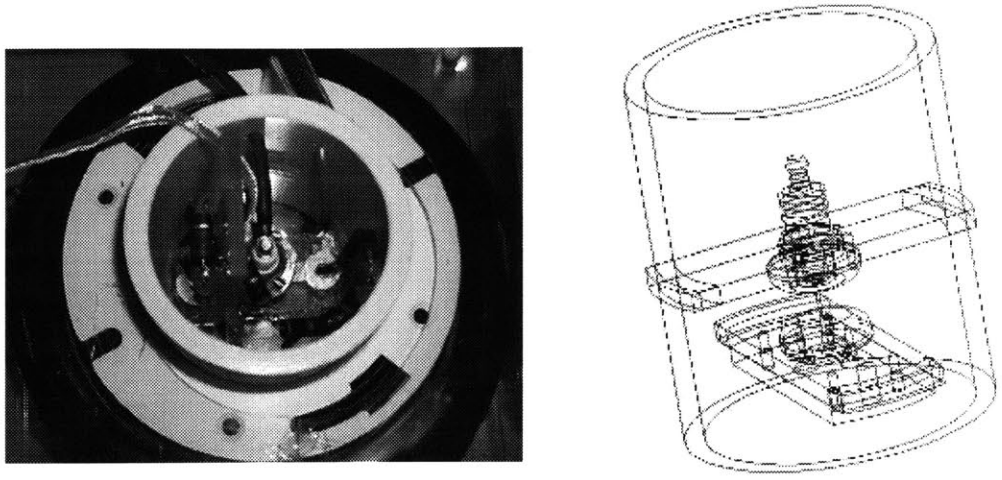

Figure 3-9 Final Version of New Triggertron

3.1.2 Complete Compact Pulser

The 2000 version of the pulser is entirely self-contained. The power supply and trigger are now inside a steel box along with the coil of charged cable. [Fig. 3-10] With a few modifications for weatherproofing, this version will likely go to the field with the test gap developed in chapter 2. The power supply is a Spellman High Voltage 0-30kv supply. The ignition for the triggertron is now accomplished by a WELLS DR-100 HEI ignition module- a compact monolithic device that replaces the large capacitive discharge unit. The ignition coil is also a more compact unit. The whole assembly runs off of 24V DC and is fed by an external universal power supply. By using a modular universal power supply, the pulser can run off of 120Vac, the station batteries, or whatever power is handy at the transformer, making installation easier. The resultant output is clean, with a good constant value. Figure 3-3 is an example of the typical output pulse.

Figure 3-10 2000 Version of Pulser. Note power supply and ignition are internal

3.2 Data Acquisition

In all versions of the NDBD system, data is gathered digitally. The breakdown measurements are taken with the Tektronics probes connected to a Tektronics TDS 220 scope with a GPIB interface. The waveforms on the scope are captured by a Macintosh G3 with a GPIB card. A customized LabView application analyzes the waveforms and determines the time to breakdown, counts the number of shots and calculates some statistics on the data. This system has worked well to gather data on over twenty oils in the laboratory, but it is too delicate, complicated and expensive for continual use in the field.

3.2.1 Analog Measurement

An alternative to the expensive digital system currently in use is based on simple analog components. The simple analog circuit shown in figure 3-11 converts the time until breakdown to a voltage across capacitor C1. Capacitors C2 and C3 act as a capacitive voltage divider of the voltage across the gap. As long as there is voltage across the gap capacitor C1 charges through diode D1. A long breakdown would allow more

time for C1 to charge up, whereas a shorter breakdown would not. The voltage on C1 is an indication of the breakdown time. The voltage on C1 can either be read by a slow and inexpensive voltmeter, or used to drive an optical coupler for a time depending on the amount of stored charge. This circuit has been constructed and tested, but has not yet been integrated into the data acquisition system. Figure 3-12 shows the capacitor voltage as a function of breakdown time. With proper choice of C1, C2, C3, and resistive load a near linear relation between time and voltage is obtained.

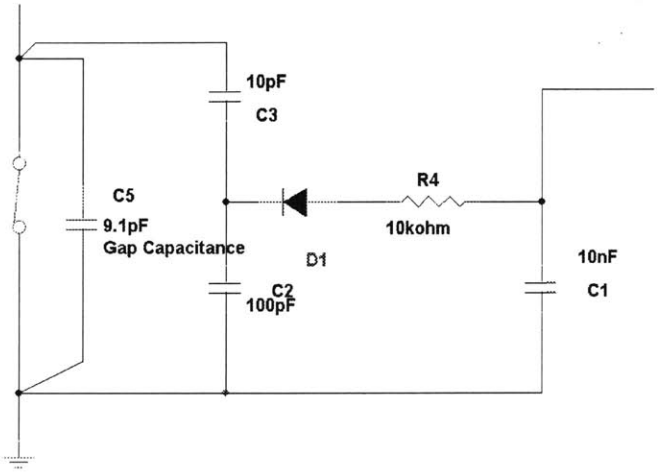

Figure 3-11 Analog time to breakdown measurement circuit

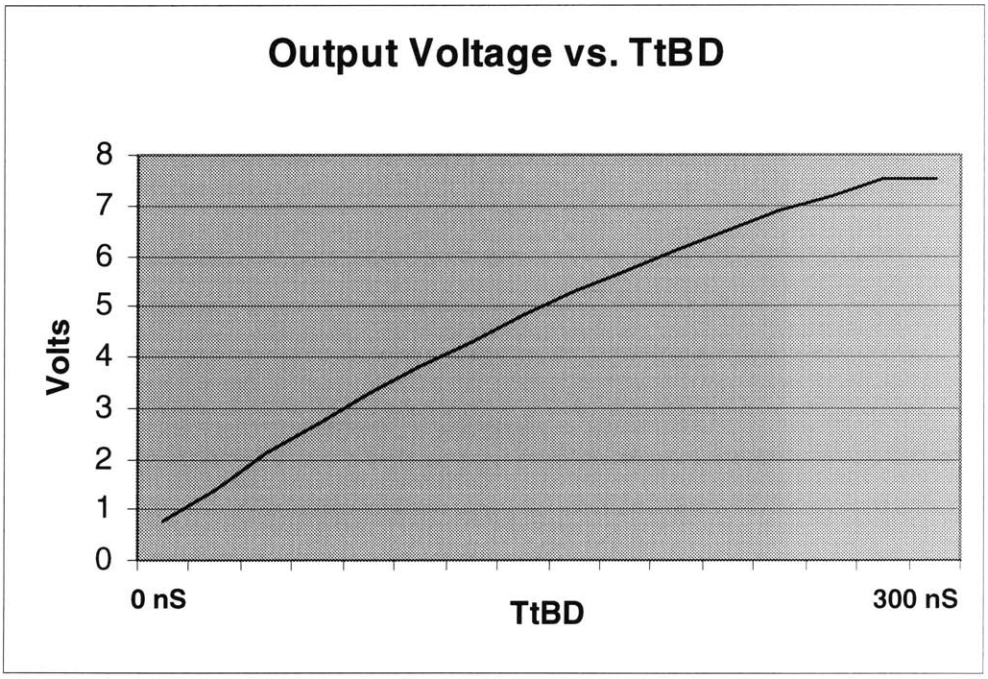

Figure 3-12 Voltage measured on C1 vs. the time until breakdown

Figure 3-13 depicts the simulated and measured analog voltage on capacitor C1 showing the rise is proportional to the time of the applied test voltage.

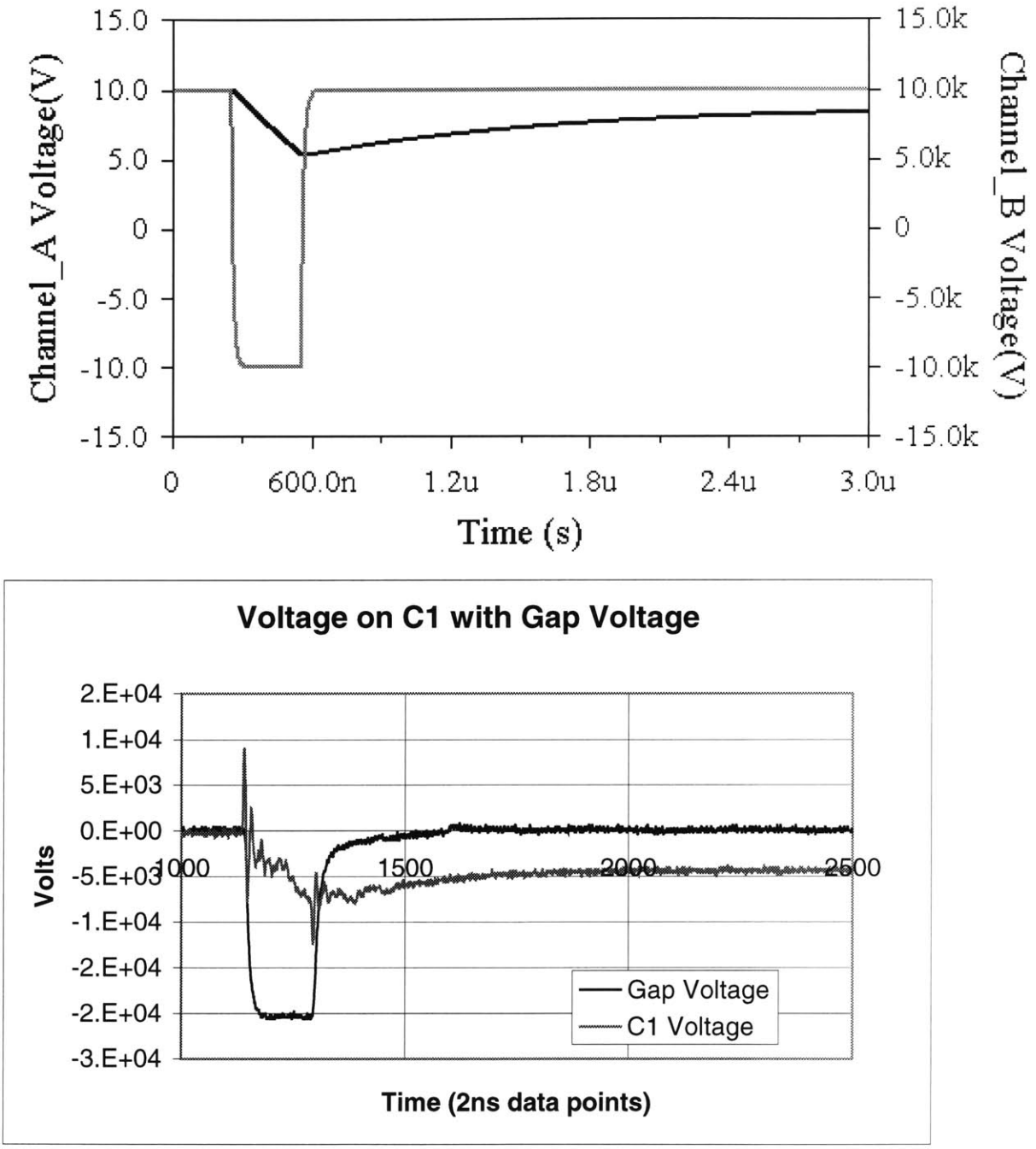

Figure 3-13 Simulated (top) and measured (bottom) analog data acquisition circuit output

Chapter 4

Oil Tests with Complete NDBD System

Using the 1999 version of the pulser and the recommended non-custom test cell outlined in chapter 2. A thorough series of test was run on over 20 oils in various conditions. Table 3 shows the result of these NDBD tests alongside ASTM D-877 results. As can be seen there is a very strong correlation between the NDBD results and the D-877 results. The NDBD test did not miss a single weak oil. These results confirm what has been shown in earlier work, [2] that the NDBD test is a viable alternative to the ASTM tests for oil condition assessment. These results also demonstrated the use of a rugged spark plug as the test gap instead of the delicate and expensive needle and plane. Thus paving the way for a probe suitable for the field.

Table 6 Test results showing both NDBD and ASTM methods

				NDBD test Volts									
	File ID Label	D-1816	D-877	20	20	20	22	22	22	24	24	24	NDBD
No.		(kV)	(kV)	BDF	TBD	BLU	BDF	TBD	BLU	BDF	TBD	BLU	recommended Action
30	EastSt+carb		25	.75	256	0.5	1	146	17	1	127	7.6	ALERT
28	E36St		32	.05	306	0.3	0.7	229	0.8	1	141	0.6	attention
22	Southport		33	.00	309	.00	.60	271	.58	1	209	4.65	watch
4	SaltdomeT1	15	36	.05	305	.40	.00	309	.00	.85	183	.80	watch
2	AddisT2	23	40	.00	309	.00	.00	309	.00	.90	212	.70	NoAction
7	GeigyT2	24	40	.00	309	.00	.00	309	.00	.10	305	.30	NoAction
6	Stauffer51	34	40	.00	309	.00	.00	309	.00	.00	309	.00	NoAction
21	9Mile	13	41	.00	309	.00	.00	310	.00	.85	252	.20	NoAction
19	GeigyT1	32	42	.00	309	.00	.00	310	.00	.80	221	.60	NoAction
1	AddisT3	34	42	.00	309	.00	.15	300	.30	.80	214	1.30	NoAction
8	PineblufD98	15	43	.05	306	.00	.00	309	.00	.95	199	.80	watch
16	AddisT5	28	43	.00	309	.00	.00	309	.00	.00	309	.00	NoAction
17	PineblufD99	15	44	.00	309	.00	.00	310	.00	.95	201	1.60	NoAction
18	Irion	22	44	.00	309	.00	.00	309	.00	.85	242	2.70	NoAction
12	SaltdomeT2	31	45	.00	309	.00	.00	309	.00	.60	264	.60	NoAction
11	FancyPt14	32	45	.00	309	.00	.00	309	.00	.75	238	.50	NoAction
3	AddisT4	33	45	.00	309	.00	.00	309	.00	.95	222	.30	NoAction
10	AddisT1	26	46	.00	309	.00	.30	292	.20	.95	196	1.80	watch
9	FancyPt11	32	46	.00	309	.00	.00	309	.00	.85	231	.30	NoAction
13	Montrose	34	48	.00	309	.00	.00	309	.00	.00	310	.00	NoAction
20	BradyhtsT1	36	48	.00	309	.00	.00	309	.00	.75	229	.90	NoAction
5	SaltdomeT3	22	49	.05	307	.20	.00	309	.00	.00	310	.00	NoAction
15	FancyPt13	31	49	.00	309	.00	.50	277	.40	.80	237	.40	NoAction
27	barrel-4		50	.00	309	.00	.00	309	.00	.00	310	.00	NoAction
26	barrel-3		51	.00	309	.00	.00	309	.00	.00	310	.00	NoAction
14	Stauffer52	25	52	.00	309	.00	.00	309	.00	.85	238	.50	NoAction
25	barrel-2		52	.00	309	.00	.00	309	.00	.00	309	.00	NoAction
24	barrel-1		53	.00	309	.00	.00	309	.00	.00	310	.00	NoAction

Chapter 5

Summary

The new non-destructive test of dielectric oil strength based on the NDBD methods is a promising technique to automate and make more reliable a diagnostic that presently involves intensive manual efforts. This is a good example of using modern electronics to transform an expensive laboratory test to a simple automated sensor that operates reliably in the field.

The work in this thesis was centered mainly on two areas, but also kept as a central point the practical need for a low cost reliable device. Special emphasis was given to the microscopic discharge event of the NDBD test method. Using circuit modeling and measurements, it was shown that the small amount of gas released was related to $R\int i^2 dt$, the energy transferred to the oil. Methods were proposed for minimizing the $R\int i^2 dt$ and thus any potential effect on the oil. Through the use of macro video it was shown that the micro-discharges of the NDBD method were indeed very small. Furthermore, significant microscopic motion occurs in the oil from the test pulse, and that it was not harmful to the test results. An unambiguous model for this motion could not be identified, but the amount of flow was show to be clearly correlated to the peak arc current. Further study of this oil motion after breakdown could prove very interesting. Video images show that the discharge is always physically very small and of very short duration. The power dissipated in the oil was only 10^{-5} Joules and moved only 10^{-4} Coulombs of charge.

The electronics associated with production of a fast high voltage pulse and detection of the time to breakdown was the other major focus in this work. Compact and reliable circuitry to achieve these goals was developed and for the most part tested. The development of an equivalent circuit at the nanosecond pulse level for the test gap and associated hardware was also part of this effort.

With an electrical model of effects in the oil and the new compact pulser designs, a compact and electrically sound NDBD in-situ tester can readily be designed. Only analog data acquisition remains to be integrated into the overall system.

Overall, consistent results between theory and measurement were achieved. By combining the various parts, a compact and reliable NDBD test device was demonstrated and shown to yield good measurements on a range of example oil samples.

References

[1] American Society for Testing and Materials, "Designation D 877-87, Standard Test Method for Dielectric Breakdown Voltage of Insulating Liquids Using Disk Electrodes", The Annual Book of ASTM Standards, ASTM, 1989.

[2] Chathan M. Cooke and Wayne H. Hagman, *Final Technical Report, A Non-Destructive Breakdown Measurement for Oil Dielectric Strength Testing*, Laboratory for Electromagnetic and Electronic Systems and Electric Utility Program, Massachusetts Institute of Technology, Cambridge, MA, April 1994.

[3] C. Mazzetti, M. Pompili, and E. O. Foster, "Study of the Time to Breakdown Under Impulse Conditions", IEEE, 1988

[4] James Hardy, *High Frequency Circuit Design,* Reston Publishing Company, 1979.

[5] A. Béroual and I. Fofana, "Modeling of the Streamer in Dielectric Liquids with an Equivalent Electrical Network", Conf. Record, 12th Intn'l Conf. On Conduction and Breakdown in Dielectric Liquids, Roma, Italy, pp.214-217, 1996.

[6] Robert G. Grzesik and Lajpat R. Utreja, "The Charge Carrier Velocity Model of The Spark Gap", Conf. Record, 7th Intn'l Pulsed Power Conference, pp.522-526, 1989.

[7] W. G. Chadband, "From Bubbles to Breakdown, or Vice-Versa",Conf. Record, 11th Intn'l Conf. On Conduction and Breakdown in Dielectric Liquids, pp.184-193, 1993

[8] V. F. Klimkin, "Bubble Generation Model for Initiating Breakdown from Anode in n-Hexane with Quasi-Uniform Electrical Fields", Proceedings of 13th Intn'l Conf. On Conduction and Breakdown in Dielectric Liquids, Nara, Japan, pp. 199-202, 1999.

[9] H. M. Jones and E. E. Kunhardt, "Development of Pulsed Dielectric Breakdown in Liquids" J. Phys. D: Appl. Phys., Vol. 28, pp. 178-188, 1995.

[10] R. Kattan, A. Denat, and N. Bonifaci, "Formation of Vapor Bubbles in Non Polar Liquids by Current Pulses", Conf. Record, 10th Intn'l Conf. On Conduction and Breakdown in Dielectric Liquids, pp.340-344, 1990

[11] Liang Chi Shen and Jin Au Kong, *Applied Electromagnetism,* PWS Publishing Company, 1995

[12] Frank M. White, *Fluid Mechanics, 3rd ed.* McGraw-Hill Incorporated, 1994.

[13] T. Takashima and R. Hanaoka, "I-V Characteristics and Liquid Motion in Needle Plane and Razor Plane Configurations in Transformer Oil and Liquid Nitrogen" IEEE Trans EI-23, No. 4, p.645, 1988.

[14] Dieter König and Y. Narayana Rao, *Teilentladungen in Betriebsmitteln der Energietechnik,* p. 89, vde-verlag gmbh, 1993

Appendix A

Video Sequence of ASTM Breakdown

Note, these video images are unmagnified and should be seen at approximately 15 times larger than the images of NDBD shot earlier in this paper.

1) Time = -33ms Before Breakdown
2) Time = 0ms Breakdown
3) Time = 33ms
4) Time = 66ms
5) Time = 100ms
6) Time = 133ms

1)

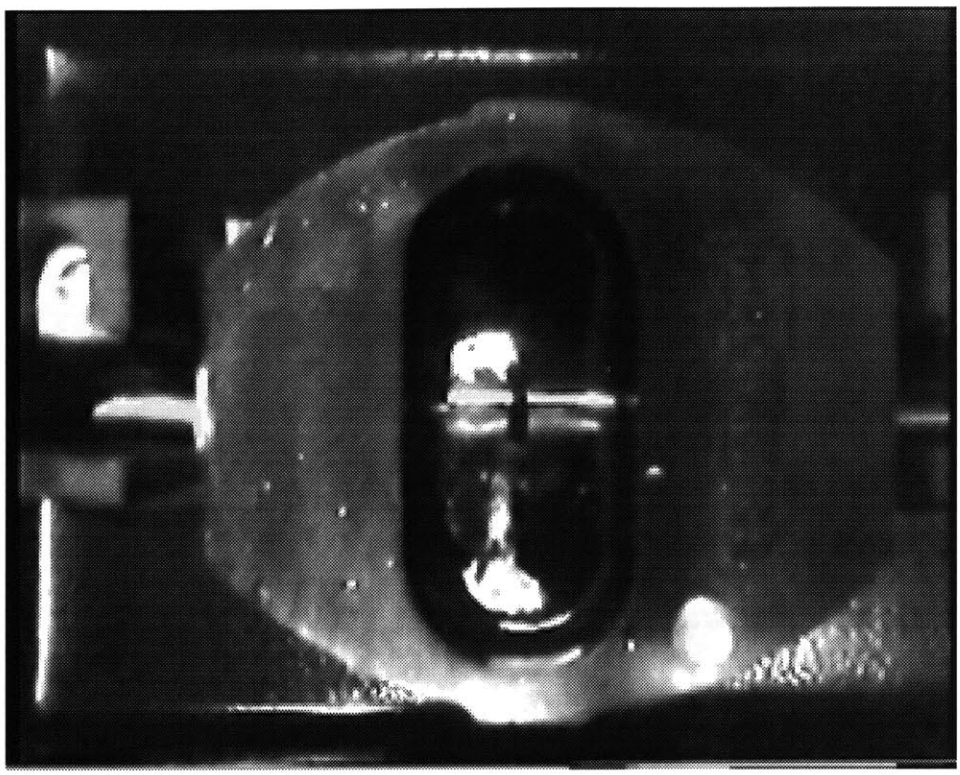

2)

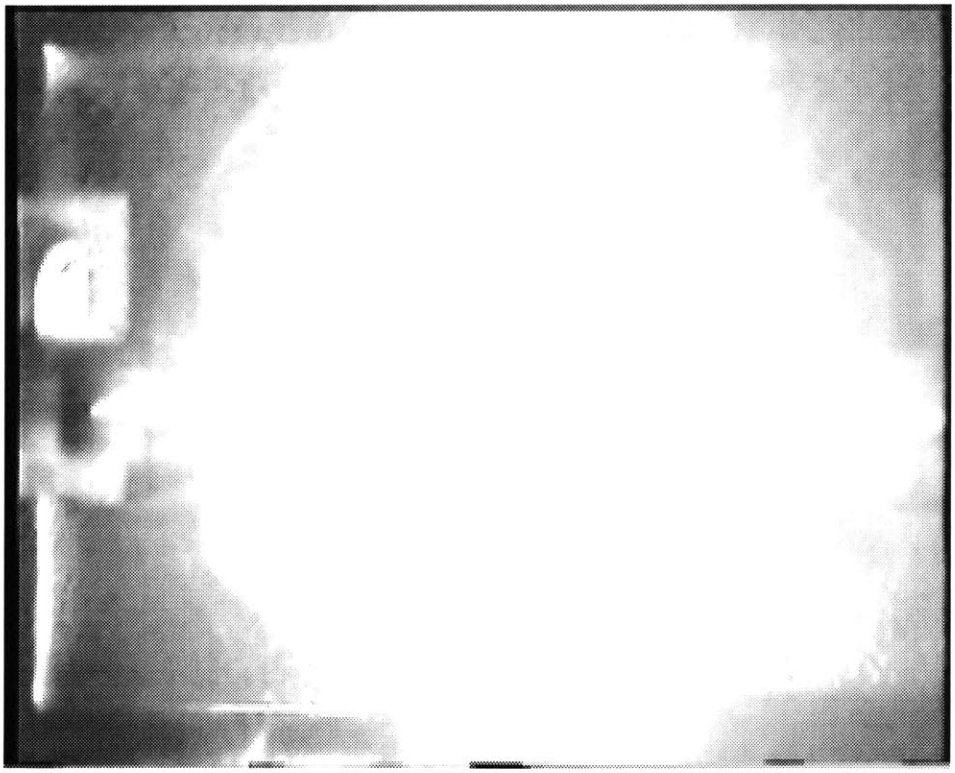

3)

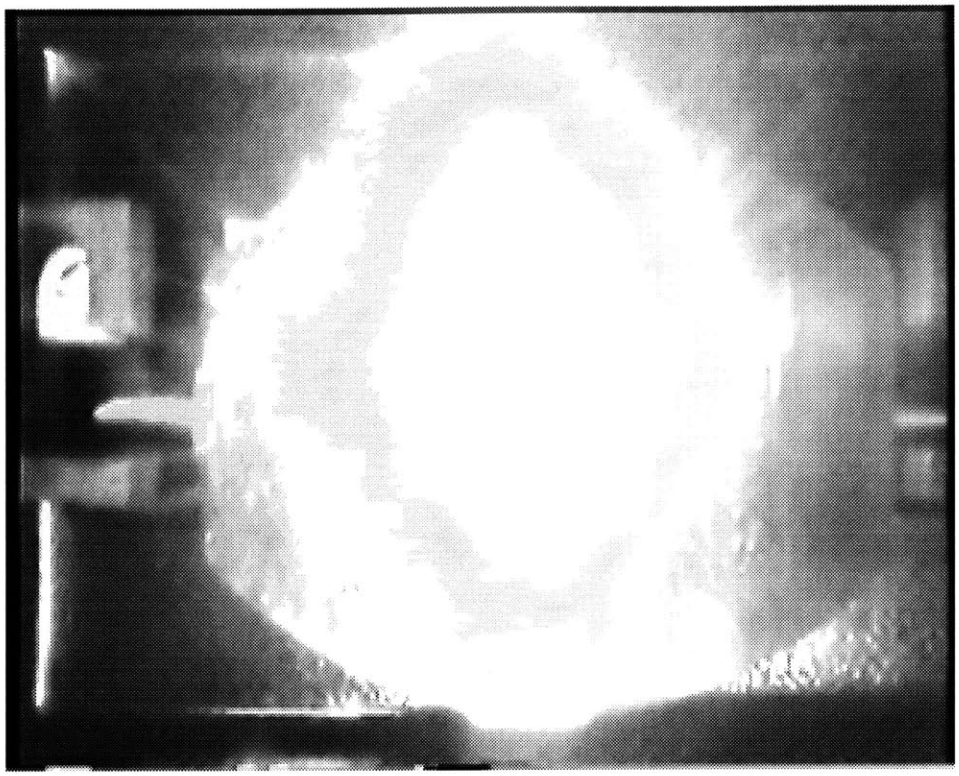

4)

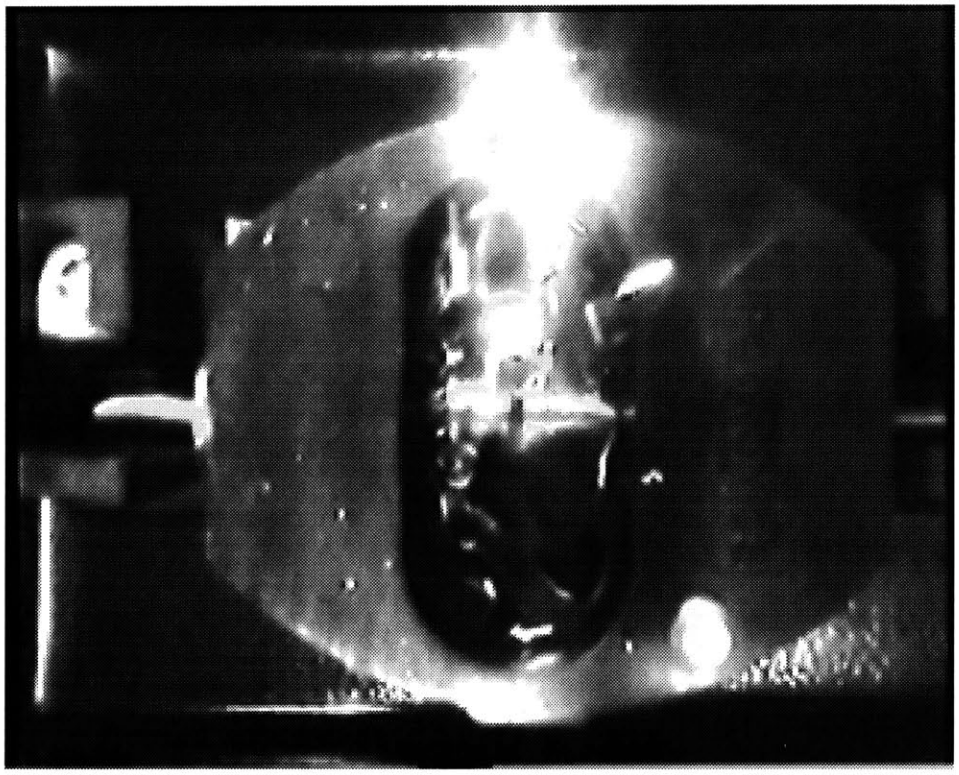

5)

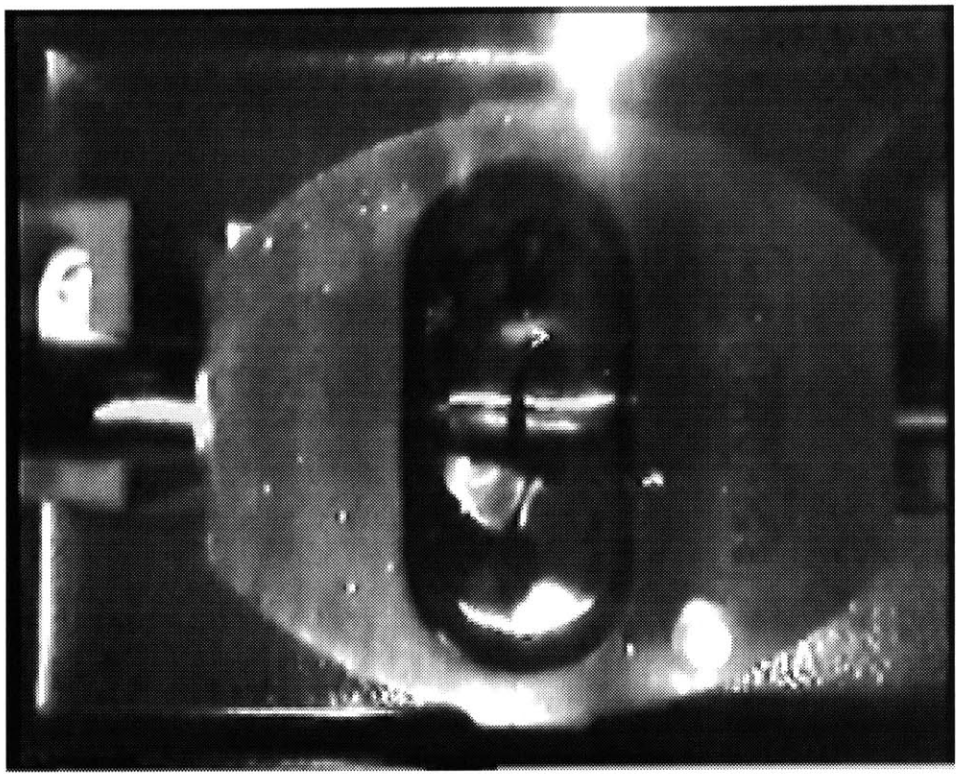

6)

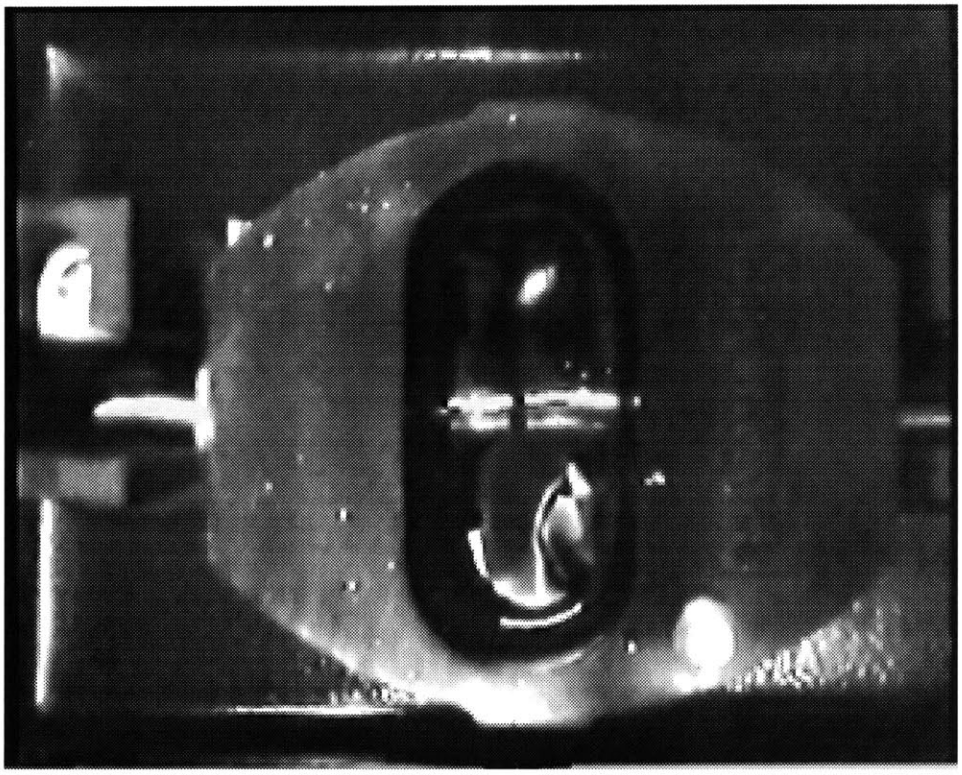

Appendix B

Derivation of Tip Volume

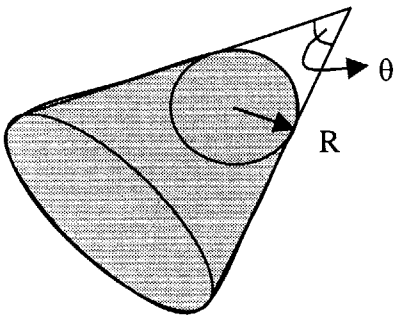

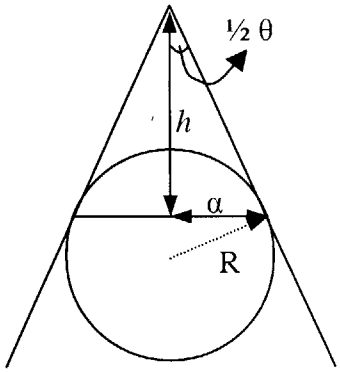

To find the volume inside a cone with a tangentially nested sphere for its bottom we will integrate in cylindrical coordinates.

$$\alpha = R\cos\tfrac{1}{2}\theta, \quad h = \frac{R\cos\tfrac{1}{2}\theta}{\tan\tfrac{1}{2}\theta} \text{ from trigonometry}$$

$$V = \int_0^{2\pi} \int_0^{\alpha} \int_{z=\sqrt{R^2-r^2}-\sqrt{R^2-\alpha^2}}^{z=-\frac{h}{\alpha}r+h} r\,dz\,dr\,d\theta$$

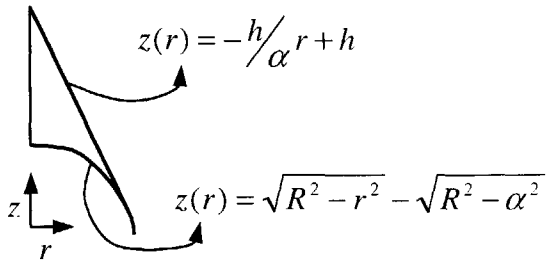

$$V = \underbrace{\tfrac{1}{3}\pi\alpha^2 h}_{\text{Volume of a Cone}} - \underbrace{\tfrac{2}{3}\pi R^3}_{\text{Volume of a Hemisphere}} + \underbrace{\alpha^2\pi\sqrt{R^2-\alpha^2}}_{\text{Volume of Cylinder inside the hemisphere}} + \underbrace{\tfrac{2}{3}\pi\left(R^2-\alpha^2\right)^{3/2}}_{\text{Piece of Hemisphere Surrounding Cylinder}}$$

Appendix C

Gallery of Video Images from NDBD Tests

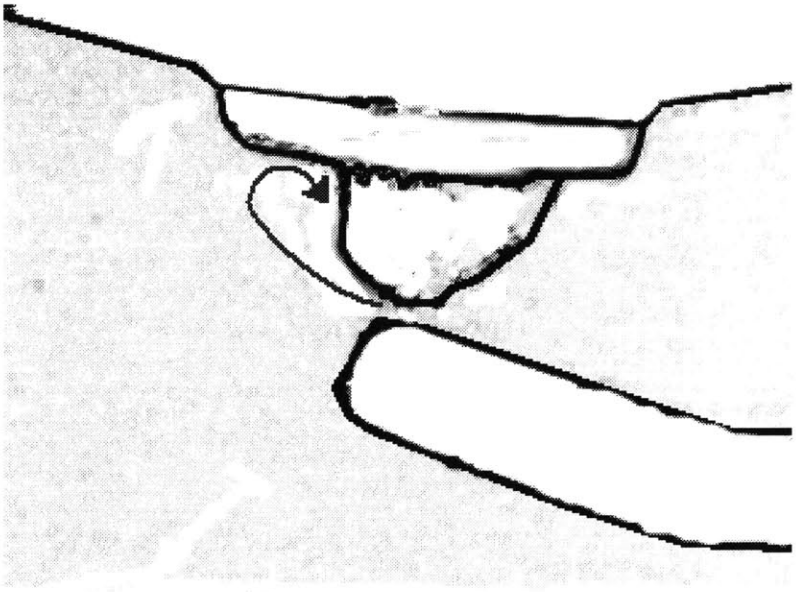

The first sequence of images demonstrates the oil flow with the motion of the micro-bubbles. The micro-bubbles happened to be caught by the flow and show the circulating motion outlined in the above diagram above over several frames Watch the tiny bubbles emerging from the gap to the left.

Time = 0ms

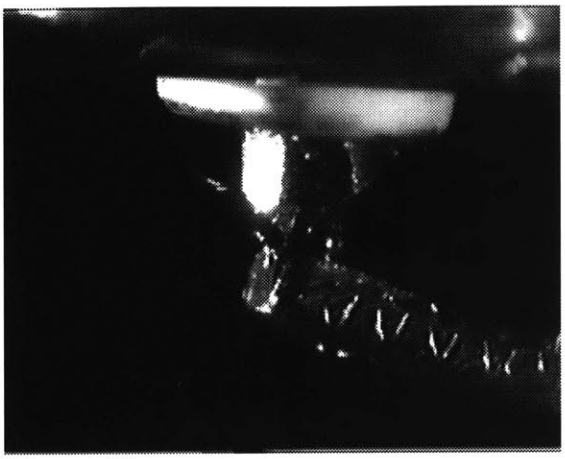

Time = 33ms

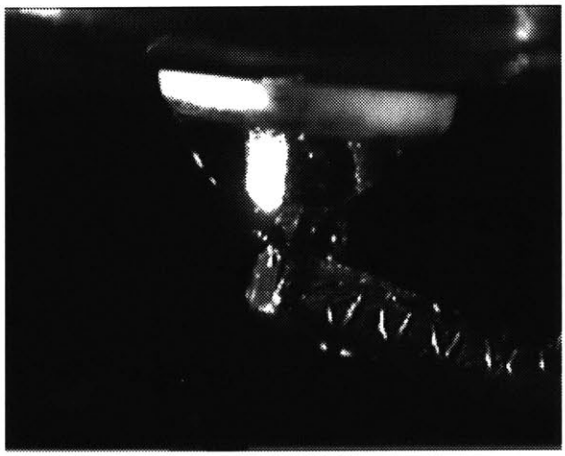

Time = 100ms

Time = 200ms

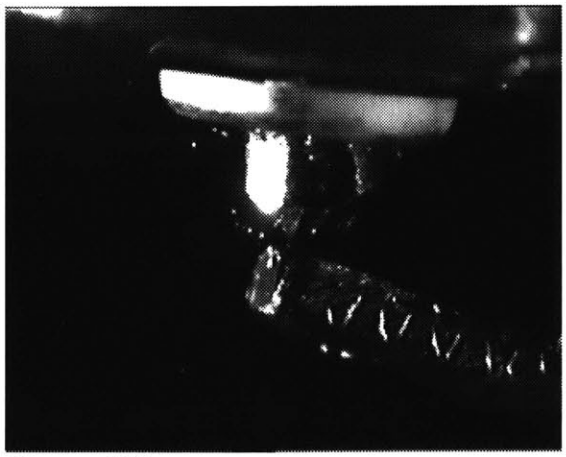

Time = 333ms

Time= 500 ms

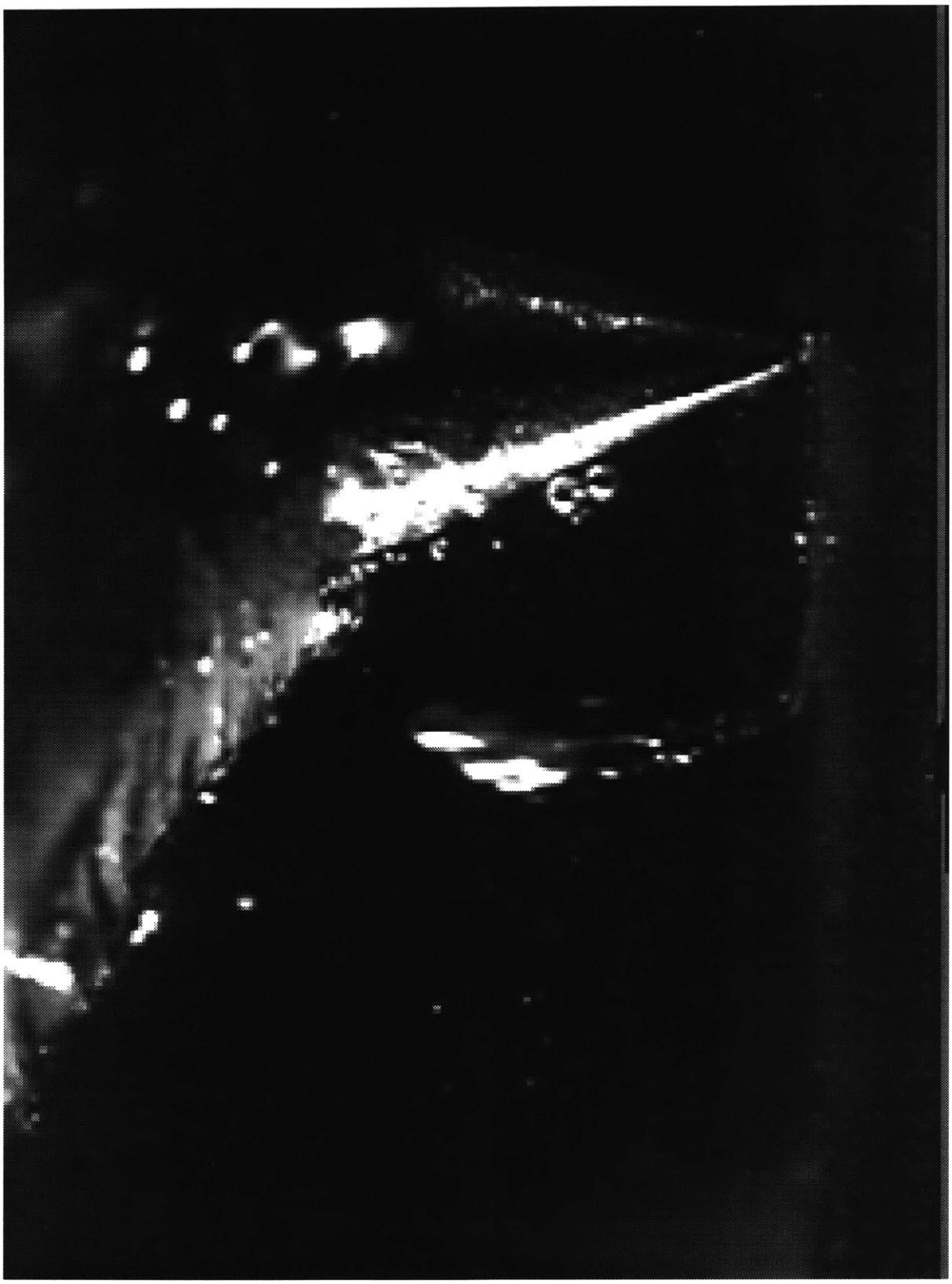

24kV, 500Ω external series resistance, Time = 266ms after breakdown

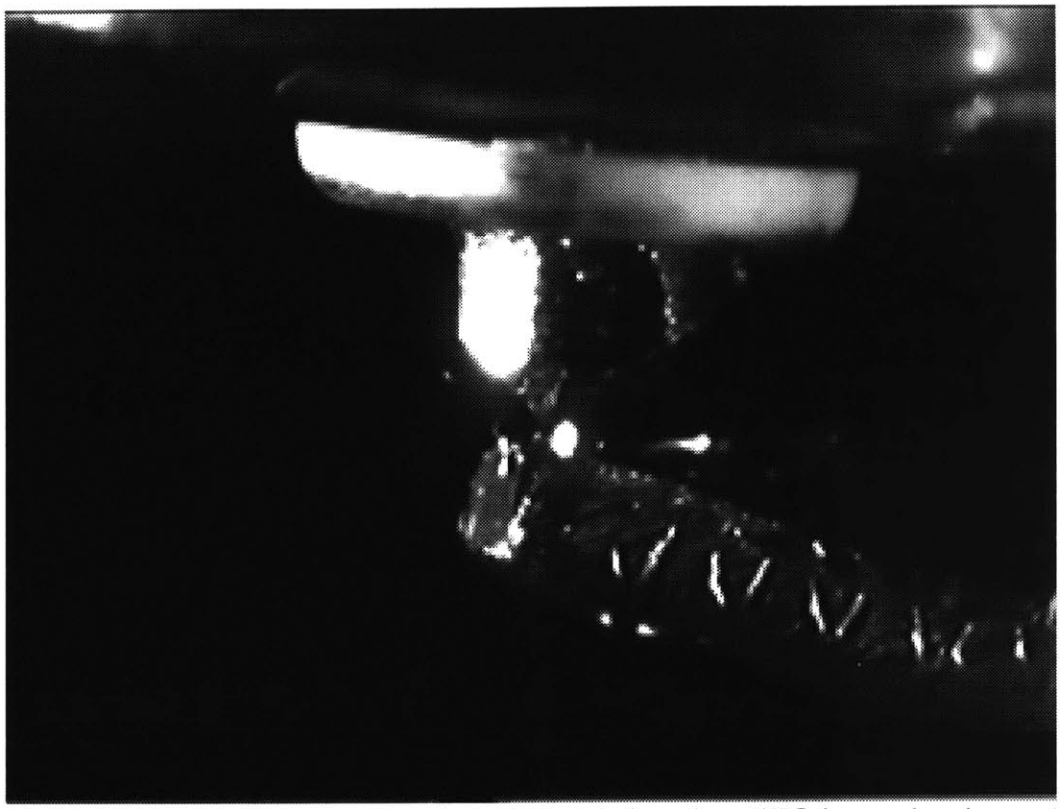

Small bubble ejected to right in AC-R45TS resistive plug (5KΩ internal resistance)

Close-up of arc in R45TS, 100x magnification, no external light- spark image only

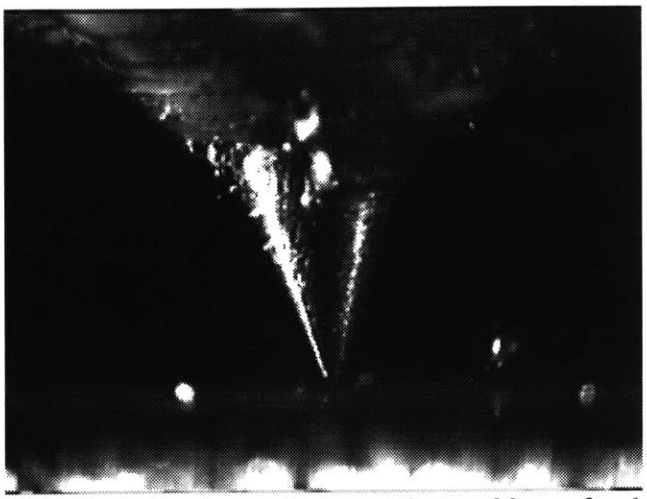

24kV, 5000Ω external series resistance, Time = 33ms after breakdown

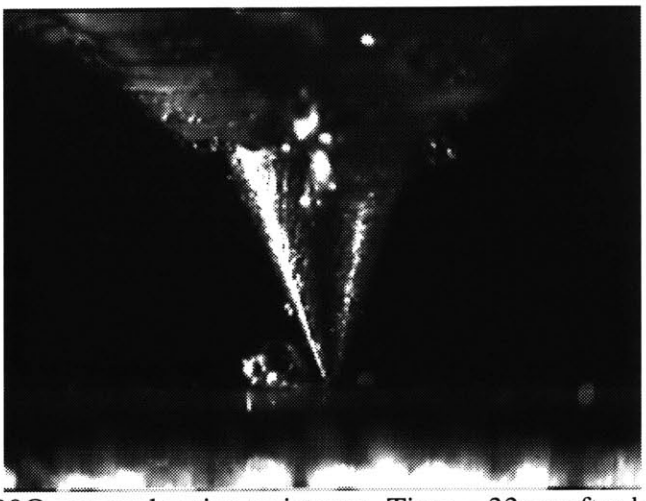

24kV, 5000Ω external series resistance, Time = 33ms after breakdown

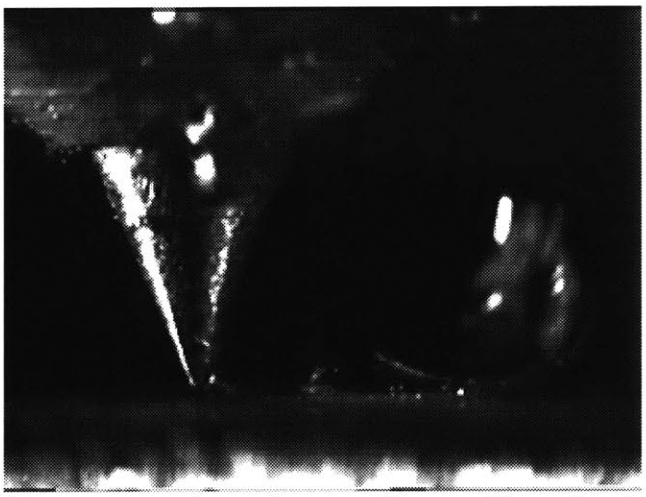

24kV, 100Ω external series resistance, Time = 66ms after breakdown

Appendix D

Example Data

The data and waveforms gathered on the 12 shots used to build the gas release model are given here.
Filenames give the voltage and series resistance and are of the format:

Date.VOLTAGE.RESISTANCE.plug.shot

FileName/Shot #	Peak I	Int I	Int I^2	RI^2	Steady I	TtBD	Gas Released	Distance Ejected
date.voltage.resistance.*	x10 Amps	Coulombs		Joules	x10 Amps	ns	cc	mm
100400.20kv.1k.NGK.017	-6.4	3.07E-06	5.01E-06	3.11E-05	-0.2	266	2.0E-06	2.0
060400.24kv.500.NGK.006	-10.0	9.12E-06	3.27E-05	1.44E-04	-4.4	169	1.3E-06	2.5
060400.24kv.500.NGK.020	-13.7	9.70E-06	3.66E-05	1.61E-04	-4.4	165	2.6E-06	1.4
060400.20kv.500.NGK.019	-11.1	4.69E-06	1.43E-05	6.29E-05	-2.9	236	2.0E-06	1.0
060400.20kv.500.NGK.020	-11.6	8.87E-06	3.12E-05	1.37E-04	-3.7	139	1.7E-06	2.8
060400.20kv.100.NGK.006	-19.6	2.24E-05	2.17E-04	3.90E-04	-13.5	188	3.1E-06	4.6
060400.20kv.100.NGK.017	-16.2	2.38E-05	2.32E-04	4.17E-04	-13.4	184	4.1E-06	2.3
060400.24kv.100.NGK.003	-21.6	2.88E-05	3.42E-04	6.15E-04	-16.1	184	5.0E-06	4.2
060400.24kv.100.NGK.015	-19.4	3.85E-05	4.88E-04	5.37E-04	-16.2	124	6.9E-06	4.4
060400.24kv.0.NGK.014	-50.8	7.07E-05	2.29E-03	2.06E-03	-47.0	203	3.2E-05	6.4
060400.24kv.0.NGK.009	-50.4	8.11E-05	2.75E-03	2.47E-03	-47.0	180	3.2E-05	4.6
060400.24kv.0.NGK.019	-51.6	7.17E-05	2.34E-03	2.11E-03	-47.4	34	2.3E-05	

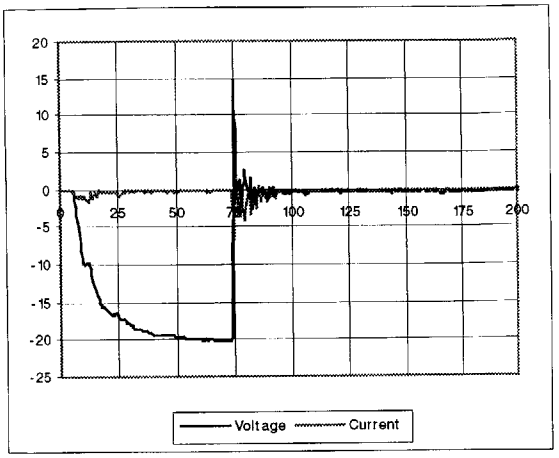

100400.20kv.1k.NGK.017

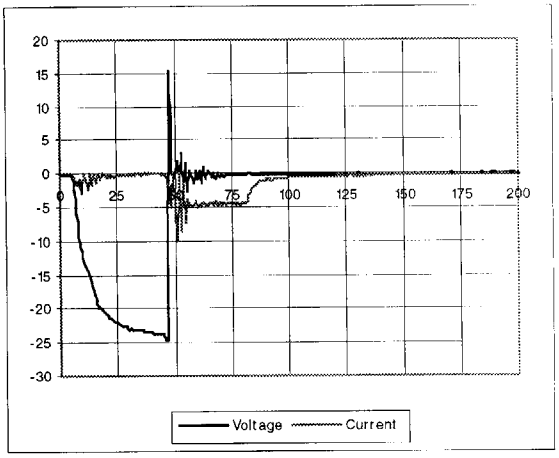

060400.24kv.500.NGK.006

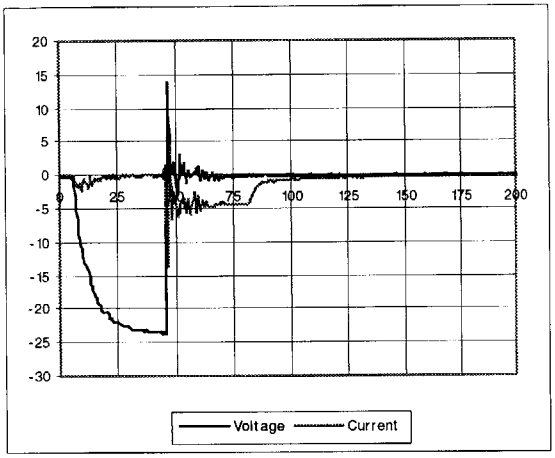

060400.24kv.500.NGK.020

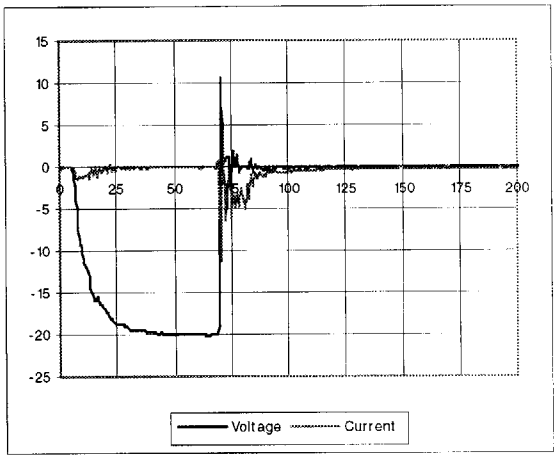

060400.20kv.500.NGK.019

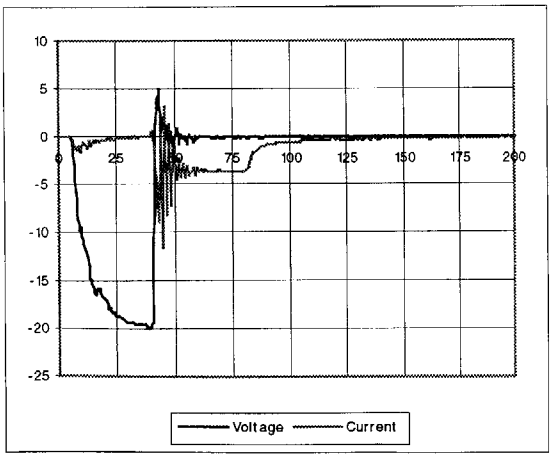

060400.20kv.500.NGK.020

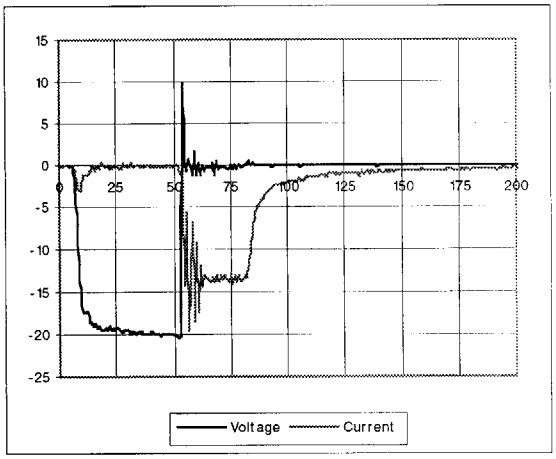

060400.20kv.100.NGK.006

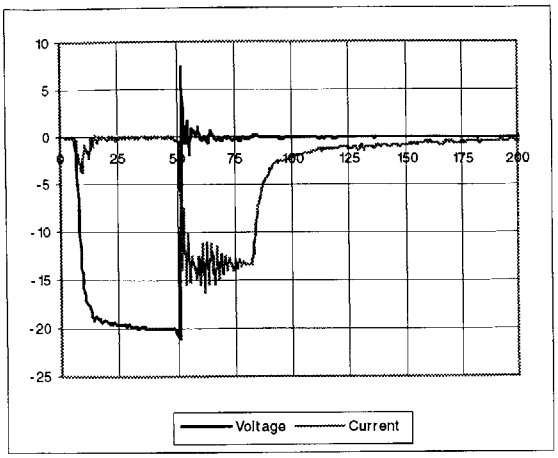

060400.20kv.100.NGK.017

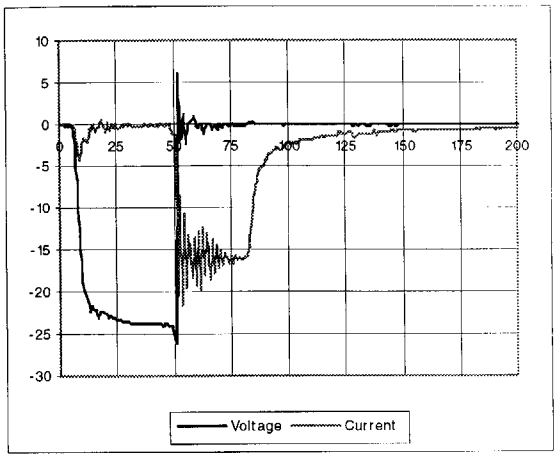

060400.24kv.100.NGK.003

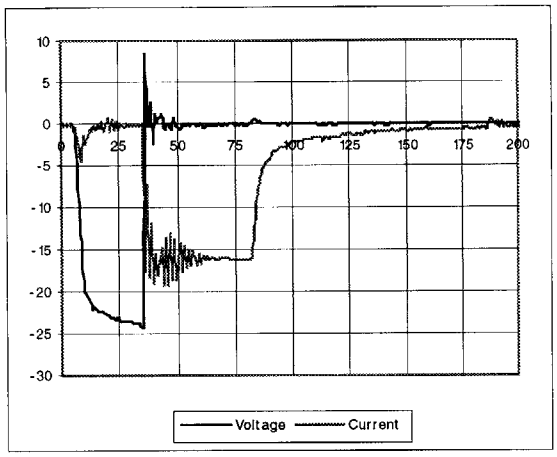

060400.24kv.100.NGK.015

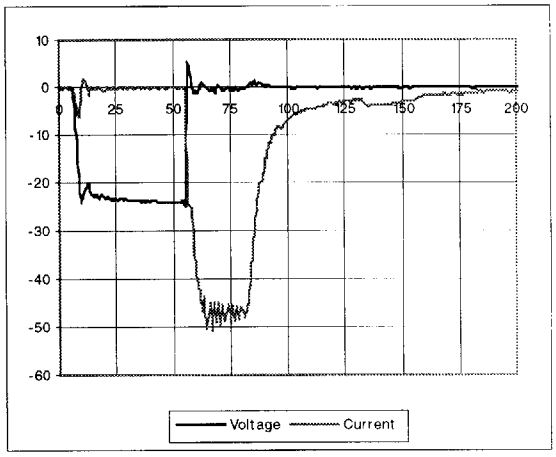

060400.24kv.0.NGK.014

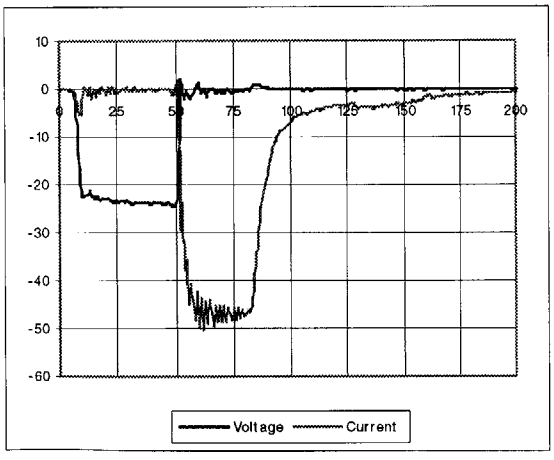

060400.24kv.0.NGK.009

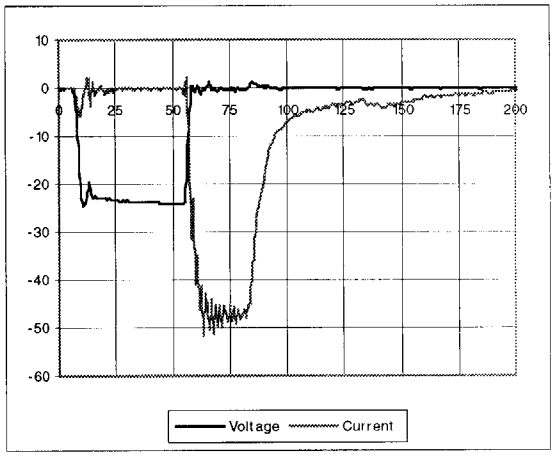

060400.24kv.0.NGK.019

Appendix E

Part Drawings for Cross-Arm Style Triggertron

These are Pro/Engineer drawings for the following parts used to make the triggertron:

1) High Voltage side electrode
2) Ground side electrode
3) Top Plate
4) Bottom Plate
5) Assembly Drawing

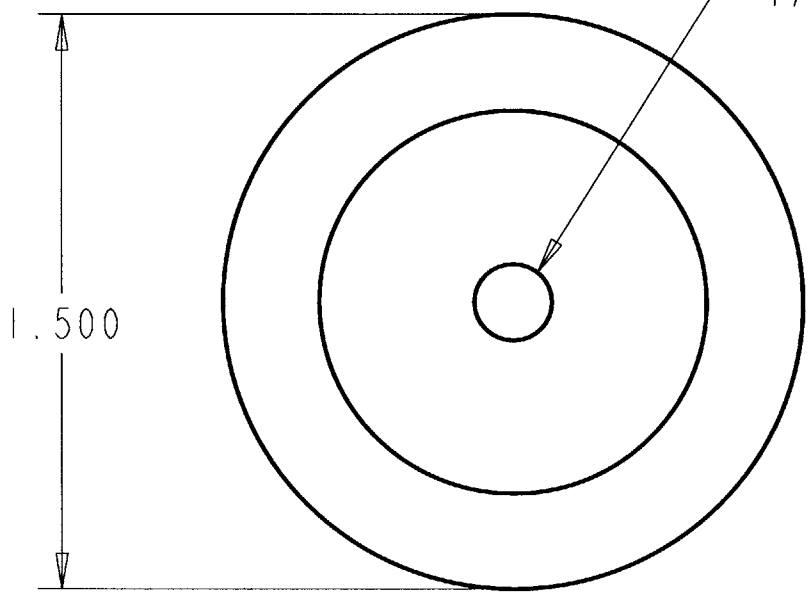

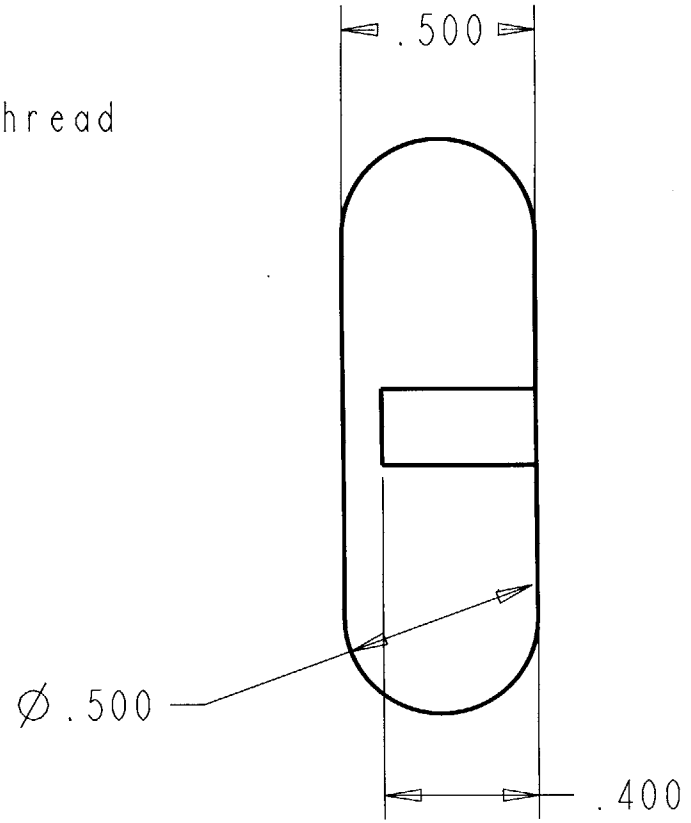

SCALE 2.000

DESIGNER 13-Jan-00 Tim	NDBD Project High Voltage Research Laboratory 155 Mass. Ave, Cambridge, MA 02139
MATERIAL BRASS	TITLE HV Side Electrode
Version 1.5" Generic Trigger	Pro/E Drawing File HV_ELECTRODE
INTERPRET PER ANSI Y14.5	
ALL DIMENSIONS IN INCHES UNLESS SPECIFIED OTHERWISE	SIZE A | SCALE 1.000 | SHEET 1 OF 1

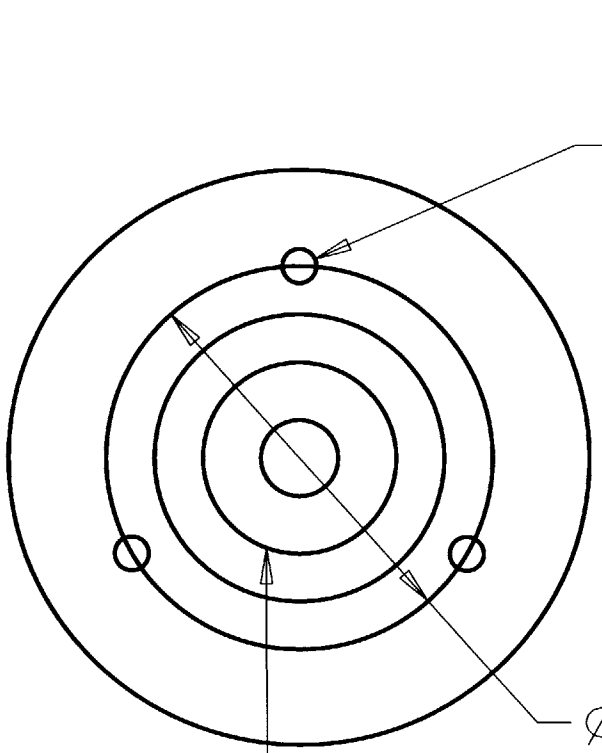

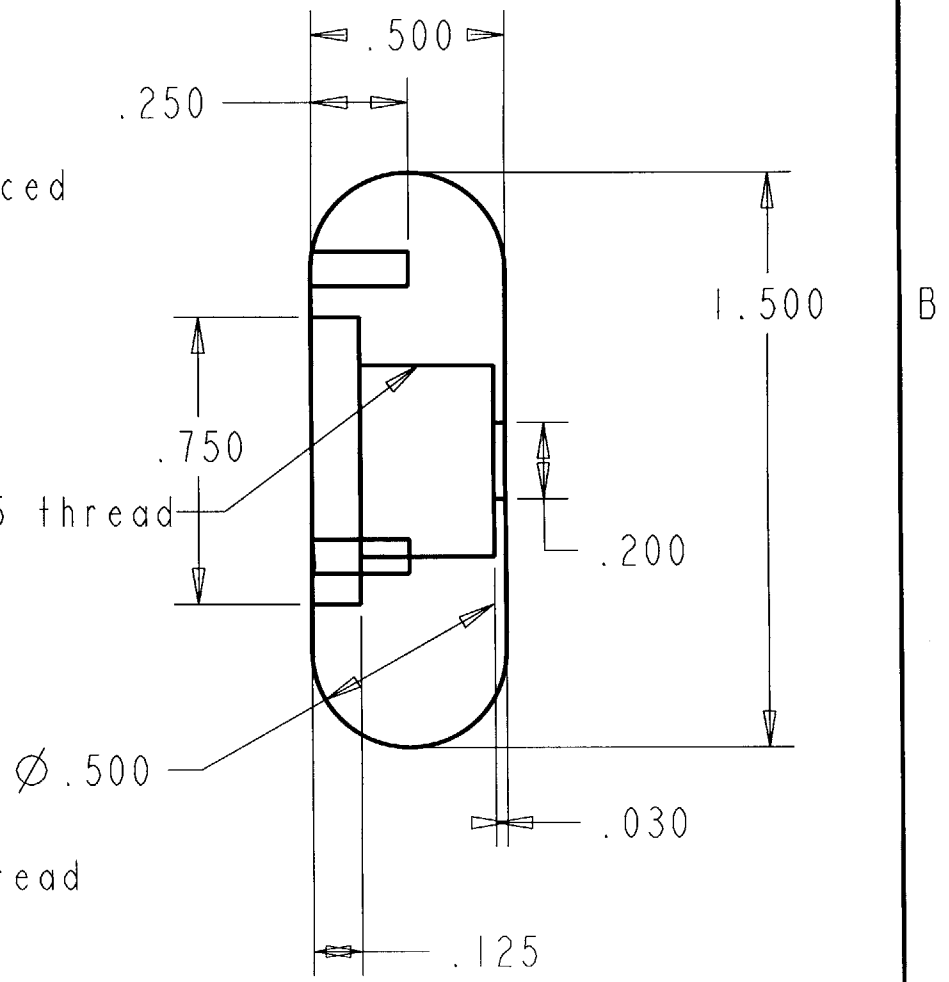

SCALE 2.000

DESIGNER 13-Jan-00 Tim	NDBD Project High Voltage Research Laboratory 155 Mass. Ave, Cambridge, MA 02139
MATERIAL **BRASS**	TITLE
Version 1.5" generic trigger	Plug Holding Electrode
INTERPRET PER ANSI Y14.5	Pro/E Drawing File PLUG_ELECTRODE
ALL DIMENSIONS IN INCHES UNLESS SPECIFIED OTHERWISE	SIZE A | SCALE 1.000 | SHEET 1 OF 1

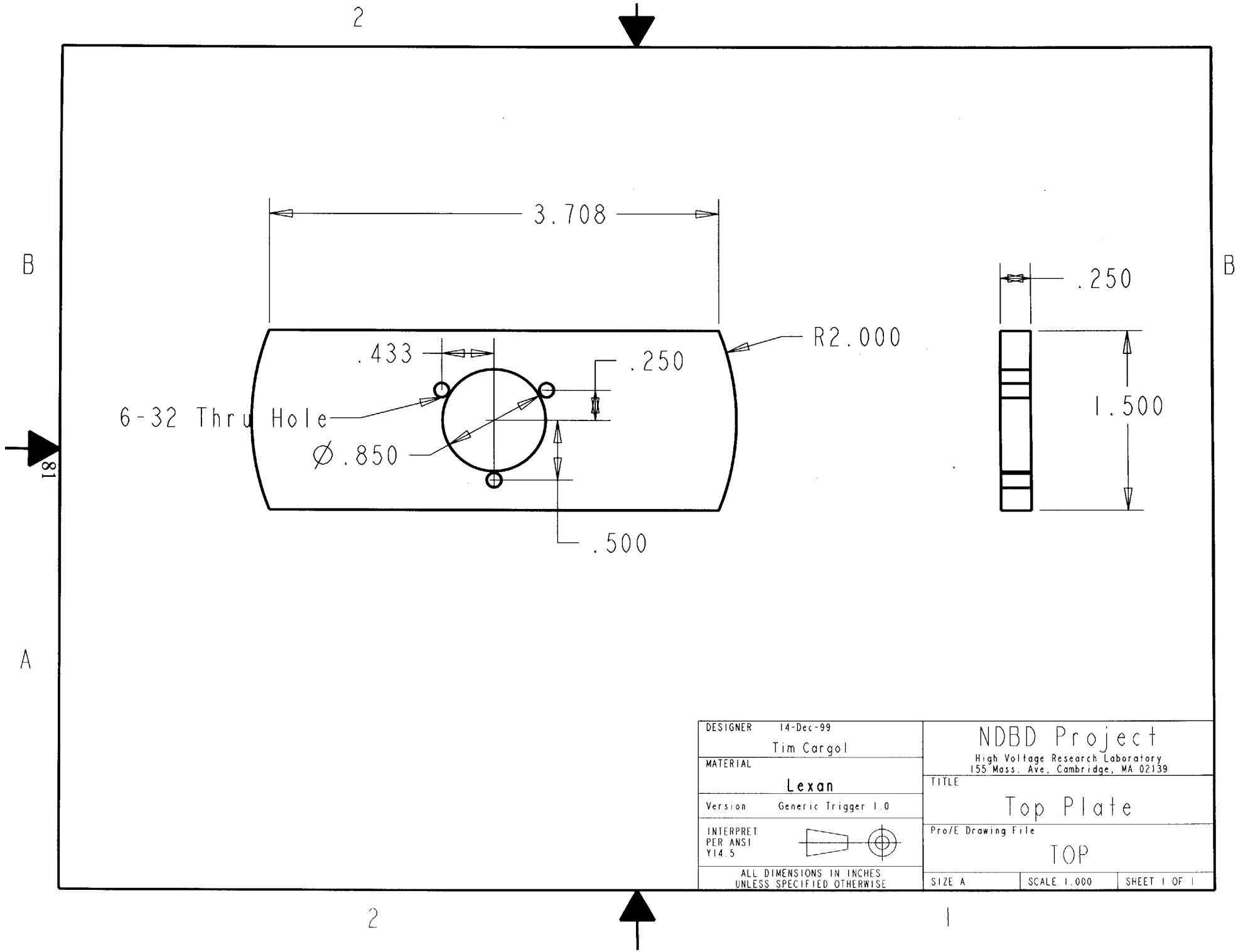

DESIGNER 14-Dec-99 Tim Cargol	NDBD Project High Voltage Research Laboratory 155 Mass. Ave, Cambridge, MA 02139
MATERIAL Lexan	TITLE Top Plate
Version Generic Trigger 1.0	Pro/E Drawing File TOP
INTERPRET PER ANSI Y14.5	
ALL DIMENSIONS IN INCHES UNLESS SPECIFIED OTHERWISE	SIZE A | SCALE 1.000 | SHEET 1 OF 1

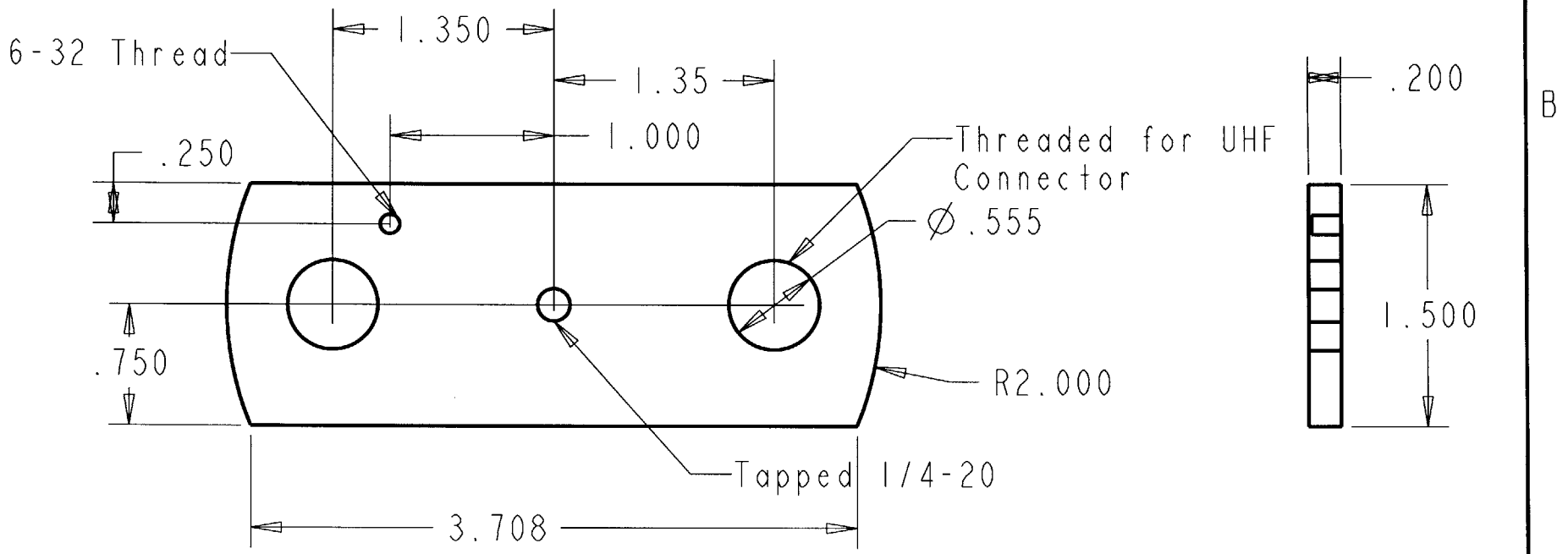

DESIGNER 14-Dec-99 Tim Cargol	NDBD Project High Voltage Research Laboratory 155 Mass. Ave, Cambridge, MA 02139
MATERIAL BRASS	TITLE Bottom Plate
Version Generic Trigger 1.0	Pro/E Drawing File BOTTOM
INTERPRET PER ANSI Y14.5	
ALL DIMENSIONS IN INCHES UNLESS SPECIFIED OTHERWISE	SIZE A | SCALE 1.000 | SHEET 1 OF 1

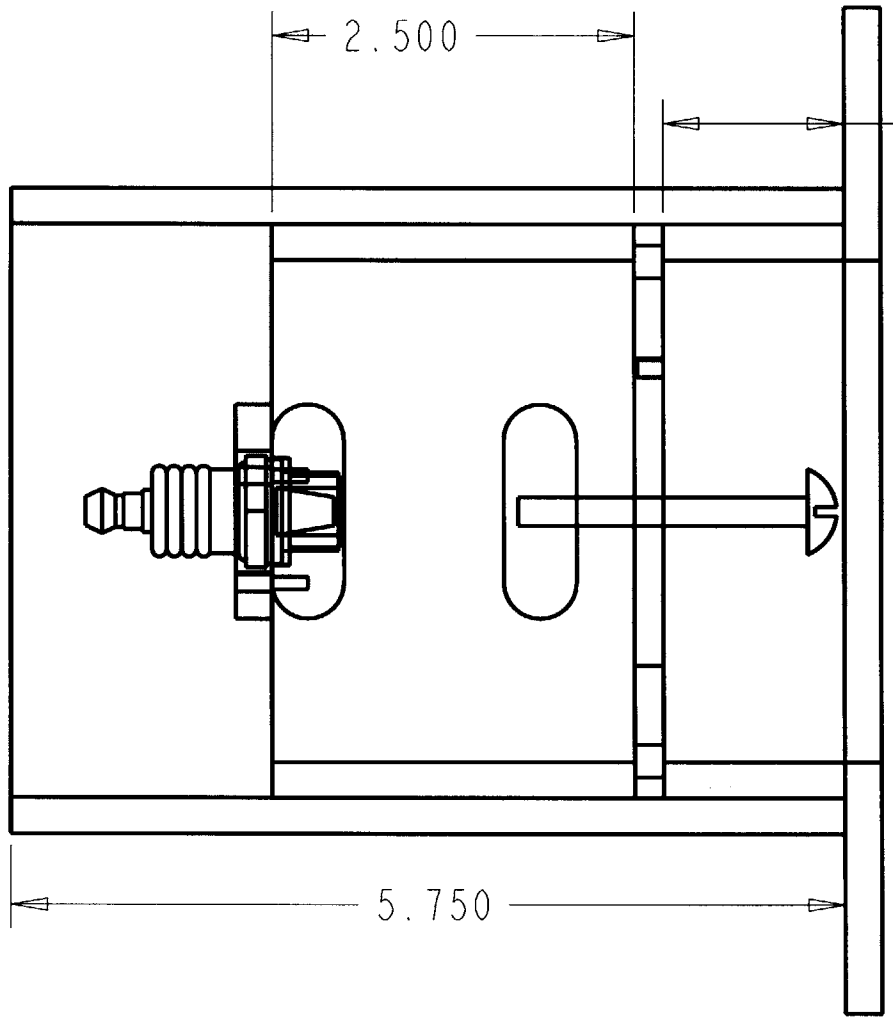

SCALE 0.750

DESIGNER 14-Dec-99 Tim Cargol	NDBD Project High Voltage Research Laboratory 155 Mass. Ave, Cambridge, MA 02139
MATERIAL PVC	TITLE Trigger View
Version Generic Trigger 1.0	Pro/E Drawing File ASSENBLY
INTERPRET PER ANSI Y14.5	
ALL DIMENSIONS IN INCHES UNLESS SPECIFIED OTHERWISE	SIZE A | SCALE 0.200 | SHEET 1 OF 1